# Cystine/Glutamate antiporter System $Xc^-$ in Beta cell and Macrophage function

**Inauguraldissertation**

zur

Erlandgung der Würde eines Doktors der Philosophie
vorgelegt der
Philosophisch-Naturwissenschaftlichen Fakultät
der Universität Basel

von

Axel de Baat

2022

Genehmigt von der Philosophisch-Naturwissenschaftlichen Fakultät

auf Antrag von

Prof. Dr. Marc Y. Donath
Prof. Dr. Christoph Hess
Prof. Dr. Daniel Konrad

Basel, den 21.06.2022

Prof Dr Marcel Mayor
Dekan der Philosophisch-Naturwissenschatlichen Fakultät

# 1. Abstract

Hormonal regulation of blood glucose is a complex dynamic process in which insulin is a major player. Beta cells are the insulin producing cells located in the pancreatic islets of Langerhans. These cells are optimized to be the perfect glucose sensors because of their specialized glucose metabolism. This optimization comes at the cost of sensitivity to reactive oxygen species, a by-product of metabolism, through relative lack of buffering capacity and high metabolic rate. Cells have systems for mitigating oxidative insults, mostly involving redox chemistry using sulphur peptides as co-factors. Upon oxidative stress, cells upregulate the light chain of system $Xc^-$, encoded by *Slc7a11*. This non-sodium dependent antiporter exports glutamate and imports cystine, the oxidized dimeric form of the semi-essential sulphur amino acid cysteine. When cysteine enters the cell, it is immediately reduced and accessible for incorporation into thiol peptides such as glutathione, used as co-factors for redox maintenance. In this study we describe the metabolic implications of *Slc7a11* deficiency in both whole body and macrophage specific knockout mice. Lack of *Slc7a11* leads to drastically lowered glutathione levels in the pancreatic islets and a defect in insulin secretion both *in vitro* and *in vivo*. We also observe a compensatory increase in insulin sensitivity that is abrogated upon dietary challenge. We find system Xc is rapid upregulation in response to lipopolysaccharides in addition to a defective cytokine production in *Slc7a11* deficient macrophages *in vitro*. We did not find a decrease in insulin secretion during myeloid specific deletion of *Slc7a11*, which excludes macrophages from driving earlier reported excitotoxicity. These findings suggest an important role for cysteine and glutathione in beta cell biology and macrophage function, with macrophage *Slc7a11* not playing a major role in the islet micro-environment.

# 2.Table of contents

# 3. List of abbreviations

| | |
|---|---|
| 2-OG | 2-Oxoglutarate |
| ATM | Adipose Tissue Macrophage |
| ATP | Adenosine Tri-Phosphate |
| AUC | Area Under the Curve |
| BMDM | Bone Marrow Derived Macrophages |
| CoA | Co-enzyme A |
| CoQ | Ubiquinone (Co-enzyme Q) |
| eAT | epidydimal Adipose Tissue |
| ETC | Electron Transport Chain |
| GGC | γ-Glutamyl-Cysteine |
| GGT | γ-Glutamyltransferase |
| GSH | Reduced Glutathione |
| GSIS | Glucose Stimulated Insulin Secretion |
| GSSG | Oxidized Glutathione dimer |
| HAT | Heteromeric Amino acid Transporter |
| ipGTT | intra-peritoneal Glucose Tolerance Test |
| ISC | Iron Sulphur Clusters |
| ITT | Insulin Tolerance Test |
| LPS | Adenosine Di-Phosphate |
| M0 | Unpolarized macrophage |
| M1 | Macrophage polarized with LPS |
| M2 | Macrophage Polarized with IL-4 |
| Mox | Macrophage Polarized with oxPAPC |
| OCR | Oxygen Consumption Rate |
| oxPhos | Oxidative phosphorylation |
| PM | Peritoneal Macrophage |
| PPP | Pentose Phosphate Pathway |
| PHD | prolyl hydroxylase domain protein |

| | |
|---|---|
| ROS | Reactive Oxygen Species |
| SSZ | Sulfasalazine |
| sXc | sysem $Xc^-$ |
| T2D | Type 2 Diabetes |
| TCA | Tri-Carboxylic Acid |

# 4. Introduction

## 4.1 Mitochondria

During the early evolutionary stages of life there was no oxygen in the atmosphere, elevated oxygen levels are measured only in samples dated as early as 2.33 million years ago[1]. Once oxygen became more abundant through photosynthesizing cyanobacteria, cells co-opted the relatively reactive oxygen to supercharge their metabolism. This phenomenon ultimately led to the endosymbiotic events that birthed the eukaryotic cell and its mitochondria[2]. Mitochondria are cell organelles, with their own genome and ribosomes, underlining their endosymbiotic origin. Structurally, mitochondria are encased in a double phospholipid membrane. The outer membrane, facing the cytoplasmic side contains many porin protein complexes that make it permeable to molecules up to 5 kD[3]. These properties allow for free flow of metabolites and products of mitochondrial metabolism among the intermembrane space between the two mitochondrial membranes and the cytoplasm, while creating a barrier for larger molecules such as proteins.

The inner mitochondrial membrane is much less permeable and contains specific transporters that maintain a tightly regulated balance of metabolites and products of mitochondrial metabolism, which is catalysed by enzymes anchored to the inner membrane. In order to maximize surface area, the inner mitochondrial membrane is shaped in folds called cristae. Some of the enzymes anchored in the mitochondrial membrane transport protons outside of the space encapsulated by the inner mitochondrial membrane, called the matrix.

Mitochondrial metabolism and structure is very reminiscent of bacteria, both utilizing a proton gradient to drive energetically unfavourable reactions[4]. Utilizing mitochondria can make eukaryotic cells up to 19x more efficient at generating adenosine tri-phosphate (ATP) from glucose. ATP is the main energy-rich co-factor of the cell that is mainly generated in mitochondria, by harnessing the tri-carboxylic acid (TCA) cycle and electron transport chain (ETC).

## 4.2 Oxidative Phosphorylation

Oxidative phosphorylation (oxPhos) is performed through the TCA cycle, which is a circular metabolic pathway that reduces NADH from $NAD^+$ by oxidizing TCA to oxaloacetate. Oxaloacetate can then be converted back into TCA by the addition of acetyl-Co-enzyme A (CoA), which is generated from the glycolysis product pyruvate. This allows the TCA cycle to be fuelled by glycolysis by regenerating TCA in a reaction catalysed by Citrate synthase. Additionally, there are many metabolic pathways leading in and out of the TCA cycle making it a central hub for eukaryotic metabolism.

TCA, also known as citrate, is converted to cis-aconitate and subsequently isocitrate by aconitase in the first step of the cycle. Isocitrate dehydrogenase oxidizes isocitrate to 2-Oxoglutarate (2-OG), generating NADH in the process and producing $CO_2$. 2-OG can additionally be anaplerotically sourced from glutamate by glutamate dehydrogenase[5]. The subsequent reaction converting 2-OG to Succinyl-CoA is catalysed by alpha-ketoglutarate dehydrogenase, consuming free Co-enzyme A and producing NADH in addition to $CO_2$. Succinyl-CoA is then converted by Succinyl-CoA synthethase to succinate, producing free CoA and generating a nucleotide tri-phosphate such as: ATP or GTP in the process. Succinate dehydrogenase doubles as complex II in the ETC, serving as the link between the ETC and oxPhos. It catalyses the conversion of succinate to fumarate, reducing its co-factor FAD to $FADH_2$. The electrons captured in $FADH_2$ are then transported further down

the ETC[6]. Fumarate is then converted to malate by Fumarase. Malate dehydrogenase converts malate to oxaloacetate, also generating NADH. Since the TCA cycle has produced two $CO_2$ molecules in one round, these two lost carbons have to be reclaimed to complete the cycle. The last step combines the final product of the cycle, oxaloacetate, with the two carbons of acetyl-CoA. This reaction results in the starting product citrate and free CoA, restarting the cycle. Additionally oxaloacetate can be generated by carboxylating pyruvate, creating an anaplerotic reaction preventing a bottleneck caused by lack of oxaloacetate availability[7].
The NADH generated by the TCA cycle can then be used by the ETC to create a proton gradient by pumping protons out of the mitochondrial matrix.

## 4.3 Electron transport Chain

The electron transport chain consists of a series of multiprotein complexes that use iron sulphur clusters (ISCs) to convert electrons from reducing equivalents and oxidation reactions into a proton gradient. ISCs are molecular composites of sulphur and hydrocarbon that stabilize iron molecules for use in catalytic sites of enzymes and hemoglobin[8]. Most of the ISCs are also sensitive to oxidation, allowing for redox mediated inactivation of ISC containing enzymes.
The mammalian electron transport chain is composed of complexes I-IV. To facilitate movement of electrons between the complexes, ubiquinone (CoQ) and cytochrome C are utilized as electron transporters. Two complexes are able to generate electrons and therefore suitable as starting points for the ETC: complex I, that oxidizes NADH to $NAD^+$ and complex II, that oxidizes succinate to fumarate and also functions as succinate dehydrogenase in the TCA cycle.
Electrons generated from both these complexes are used to reduce CoQ to $QH_2$ for transport to complex III. Complex III oxidizes $QH_2$ and uses the electrons for pumping more protons and reducing cytochrome C. Cytochrome C then transports one electron to complex IV that finally donates it to oxygen, creating $H_2O$ and pumping out more protons.
The stoichiometry of electron mediated proton transport were first theoretically determined as 4:2:4 protons per 2 electrons for complex I,III,IV respectively[9]. Empirical approaches have shown however that Complex I only transports 3 protons across the mitochondrial inner membrane[10]. Complex II does not transport protons with its activity.
The subsequent release of this proton gradient by ATP synthase powers the synthesis of ATP from adenosine di-phosphate (ADP) and inorganic Phosphate, consuming 3.7 protons in theory[11]. The eukaryotic ATP synthase utilizes 8 protons to turn the octameric ring structure of ATP synthase one revolution, which generates 3 ATP molecules. After accounting for the import ADP and inorganic phosphate, a single molecule of ATP will require the transport of 3.7 protons[12].
The proton gradient can also be used to exchange between the reducing equivalents NADH and NADPH. This is done by NNT, which is anchored to the mitochondrial membrane and transports out a proton upon conversion[13].
Uncoupling proteins also populate the mitochondrial inner membrane that release protons without performing any obvious action, which can function as a release valve for the proton gradient, leading to the generation of heat[14].

## 4.4 Reactive oxygen species

Inefficiencies in the ETC lead to leakage of electrons that can then interact with oxygen, generating superoxide. About 0.2-2% of the electrons are leaked, which means there is a steady production of superoxide associated with mitochondrial activity[15]. Superoxide is

mainly produced by complex I, II and III, and the generation is increased when flow through the cycle is overfed, reversed or halted.
Superoxide has to be quickly neutralized by superoxide dismutase to $H_2O_2$ because superoxide will oxidize metals like iron-sulphur clusters that are located in the catalytic sites of ETC complexes[16]. $H_2O_2$ is still highly reactive and when accumulated, can peroxidise lipids or generate highly toxic hydroxyl radicals through the Fenton reaction, which is catalysed by iron[17]. Glutathione peroxidase enzymes therefore detoxify $H_2O_2$ and lipid peroxides, using glutathione (GSH) as a co-factor[18]. When redox buffering fails, these reactive oxygen species (ROS) accumulate and lead to cellular dysfunction. In order to reap the benefits of including oxygen in its metabolism, organisms have to maintain a tight control over ROS levels within the cell.
By stacking feedback loops, the metabolic system maintains tight control over metabolic activity. Feedback is when an output of part of a causal chain modulates the activity in a different part of the chain. In the context of metabolic pathways this is mostly done by allosteric regulation of enzymes. Allosterism is when non-substrate products modulate enzyme activity. This allows enzymes to not only sense their substrates and products, but also further up and down in the metabolic pathways, creating an interconnected network rather than a linear chain. *In silico* modelling with experimental verification has shown that summation of feedback loops lead to more robust and perturbance resistant systems[19].

## 4.5 Glutathione

GSH is a tripeptide composed of glutamate, cysteine and glycine. GSH is oxidized into its dimeric form upon its use as a cofactor. Oxidized GSH (GSSG) can then be regenerated by GSH reductase, consuming NADPH that is sourced from, Malic Enzyme 1[20], Nicotinamide Nucleotide Transhydrogenase[13] or the catabolism of glucose through the pentose phosphate pathway (PPP)[21]. The limiting substrate for the synthesis of GSH is cysteine, a semi-essential amino acid that can only be generated from the essential amino acid methionine through trans-sulfuration[22].
Cysteine's thiol group is biochemically useful for redox chemistry and the formation of sulphur bonds in proteins. Besides redox chemistry, the liver also uses GSH to generate adducts of toxic compounds that can then be exported out of the cell by MRP1[23]. Given the relatively oxidative potential of the extracellular space, cysteine is mostly present in its oxidized dimeric form, cystine[24].

## 4.6 Heteromeric Amino acid Transporters

Heteromeric Amino acid Transporters (HATs) are dimeric complexes comprised of a heavy chain, that is shared with other members of the protein family, and a light chain that determines the identity and metabolite specificity. The transporters all have antiporter activity and the family covers most cationic and neutral amino acids with most transporters covering a wide range of substrates with differing specificities. The combined activity of the family therefore contributes to the maintenance of intracellular amino acid homeostasis[25].
Cystine uptake by HATs is performed by transporters corresponding to the light chain genes: *Slc7a9* and *Slc7a11*. *Slc7a9* encodes the light chain of system $b^{o+}$ which dimerizes with a heavy chain encoded by *Slc3a1* and its expression is primarily limited to the kidney and intestinal tract.
System $b^{o+}$ imports neutral dibasic amino acids such as: ornithine, cystine, lysine and arginine. Interestingly there are inverse gradients for *Slc7a9* and *Slc3a1* expression along the renal tubule. In the proximal convoluted tubule, there is high expression of *Slc7a9* which results in high throughput low affinity cystine import. A `low-capacity, high-affinity' system, dominated by *Slc3a1* expression, is predominant in the proximal straight tubule[26].
This setup of differential uptake allows for maximum recovery of cystine. Fascinatingly, the differential expression along the renal tube suggests complex interaction between light and heavy chain that partly determine the kinetics of amino acid uptake. This effect could be mediated by light and heavy chain interactions and the dynamics of the sulphur bond connecting them. Additionally, relative abundances of the transporter substrates along the renal tubule might also have influence on the transport kinetics.
Mutations in *Slc3a1* and *Slc7a9* are associated with type A and type B cystinuria respectively that do not display a different phenotype. It has to be noted however, that heterozygous mutations of *Slc3a1* do not lead to cystinuria, whereas mutations in *Slc7a9* display varying degrees of system $b^{o+}$ substrates in the urine[27].

## 4.7 System $Xc^-$

System $Xc^-$ (sXc) is encoded by *Slc7a11,* is a relatively unique member of the HAT family as it has high specificity for cystine and exclusively exports glutamate[28]. It dimerizes with the 4F2 (CD98) heavy chain that it shares with other HATs. The transporter exchanges cystine for glutamate at a 1:1 ratio in a sodium-independent manner. In physiological conditions, the transporter exclusively imports cystine and exports glutamate. SXc is highly expressed in the brain, endocrine and sexual organs. Despite low baseline expression in most tissues, *Slc7a11* can be rapidly upregulated in certain conditions. *Slc7a11 is* upregulated upon cystine shortage by ATF4, redox stress by NRF2 and Hypoxia by HIF1-a[29]. Additionally, its transcription can be repressed by P53 during initiation of cell death, suggesting a pro-survival role[30]. The transcriptional regulation of sXc represents the dichotomous response of the cell to stress: either cope and try to survive or give up and go into apoptosis. This dichotomy is especially interesting in the context of cancer, where sXc is an important inducer of ferroptosis, an iron-dependent, peroxidated lipid mediated form of cell death that has garnered much attention in the field of cancer metabolism[31].

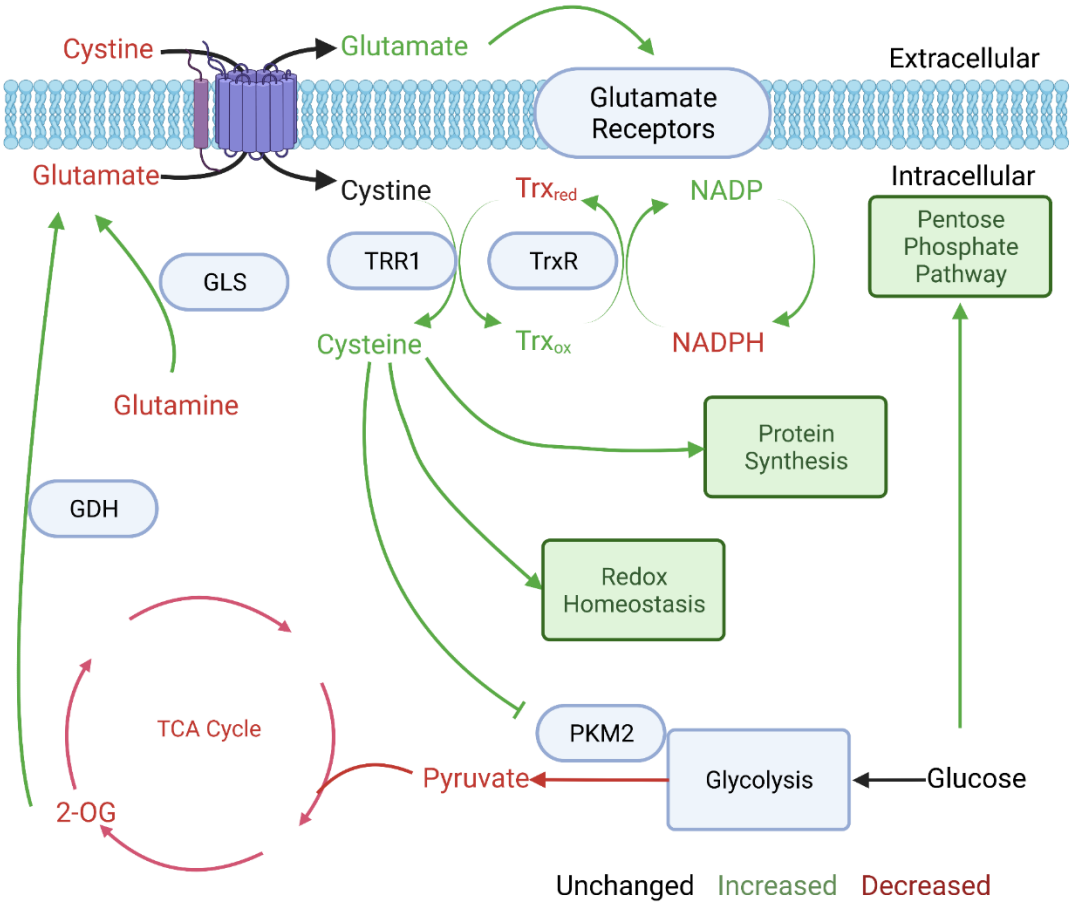


Figure 1 Metabolic implications of system Xc⁻ activity. The export of glutamate can lead to activation of glutamate sensitive receptors on the cell surface. Intracellular glutamate will be lowered and glutamate fluxes through anaplerosis from 2-Oxoglutarate and glutaminolysis. The imported cystine is rapidly reduced to cysteine, consuming thioredoxin that has to be reduced back by consuming NADPH that can lower NADPH levels, leading to activation of the pentose phosphate pathway. Intracellular cysteine then has the potential to inhibit PKM2, leading to

## 4.8 Metabolic implications of system Xc⁻ activity

Glutamate, the export product of sXc, is an important metabolite at the nexus of the TCA-cycle, amino acid synthesis and glutamine metabolism. Its activity can divert glutamate, derived from either glutamine or the TCA cycle metabolite 2-oxoglutarate (2-OG), to the extracellular space. This export of glutamate has been described to be a driver of glutamate induced neuronal cell death called “excitotoxicity”[32]. Excitotoxicity is mediated by over-activation of glutamatergic receptors on neurons by glutamate originating from glial cells. This constitutive over-excitation ultimately leads to neuronal cell death, driven by oxidative stress, excessive calcium signalling, depolarization and ultimately mitochondria mediated cell death[33].

Overexpression of sXc in cancer cells resulted in the cells becoming sensitized to glutaminolysis inhibitors which could be rescued by supplementation of 2-OG[34]. This suggests that sXc activity can markedly diminish intracellular glutamate pools, that can be replenished by anaplerosis from the TCA cycle. The reduction of imported cystine, which requires NADPH, depletes NADPH pools that needs to be replenished by the PPP[35], increasing the dependence on glucose metabolism.

When sXc is inhibited, cysteine levels within the cell rapidly drop. As a first response, the integrated stress response is activated through the GCN2-eIF2a-ATF4 axis[36]. ATF4 is a transcription factor whose transcription is upregulated when general transcription slows down[37]. Lower cysteine levels lead to eIF2a phosphorylation, which results in less transcription initiation events, that increases ATF4 expression. *Furin* deletion in beta cells has been reported to induce ATF4 mediated anabolic program that results in lower beta cell insulin output[38]. ATF4 in turn promotes the transcription of *Chac1,* encoding a glutathione degrading enzyme that responds to cysteine shortage by tapping into the GSH pool[39]. This suggests that the cell has mechanisms to prioritize protein synthesis over maintaining a large GSH pool, suggesting that GSH is not only used for redox maintenance and detoxification but also as a store of cysteine. Additionally, Chac1 serves as a safety mechanism against excessive GSH production, which mainly affects the endoplasmic reticulum with its relatively oxidative environment needed for forming protein disulphide bridges[40].

## 4.9 Cellular metabolism

Cellular metabolism could be described in essence as a dynamically stable complex system. Dynamically stable means that despite constant anabolism, catabolism and metabolic activity, the system oscillates around a certain stable point, which can be moved as a response or adaptation.
Complicated systems become complex systems when they involve too many unknowns and therefore become unpredictable.
The cellular metabolic system is based purely on interconnected chemical equilibria and diffusion through semi-permeable biological membranes. These equilibria are established by entropy and conversely enzymes catalysing energetically unfavourable reactions to create and maintain structure. These enzymes are additionally sensitive to modulation by other proteins and compounds, creating feedback loops.
Metabolic pathways in their emergent complexity maintain dynamically stable homeostasis dictated by the availability of intra- and extracellular nutrients, the anabolic demands of the cell and its environment.
Cellular metabolism is at the same time communicator and executor of cellular function, exhibiting rapid changes in response to stimuli that then lead to a functional response, facilitated by protein-based signalling pathways. Given the (semi-)stochastic nature of cellular processes, molecules, such as glucose, cannot accumulate in too high abundance without generating unwanted reactions that might interfere with cellular function[41].
Cells have therefore developed metabolic pathways to, in the case of glucose, generate glycogen as a storage that is less reactive and can readily be liberated when needed[42].
Similar mechanisms exist for iron where most iron, that serves as a co-factor for enzymes, is sequestered in ferritin. If iron is not properly stored or put into a ISC scaffold, it will serve as a catalyst to produce highly toxic hydroxyl radicals in the Fenton reaction leading to ferroptosis[43]. This way of handling reactive compounds and catalytic metals is ubiquitous within cellular metabolism. In general, cellular metabolism has to maintain two important

balances: Providing adequate nutrients for cellular process while preventing toxic accumulation and efficiently providing enough energy while not overburdening the mitochondria.

## 4.10 Multicellular organism

At some point in evolution it became favourable for cells to start cooperating at an increasingly intimate degree, leading to the first multicellular organisms. Increased specialization inherently comes with trade-offs, potentially reducing the adaptive advantage of the individual specialized cell. Collaborating with other cells that have a complementary specialization however, will allow for a synergy that has the potential to outperform unspecialized cells.

Multicellular organisms require even greater complexity for regulating the organismal metabolic homeostasis. Interconnected and overlapping balances and feedback mechanisms for each metabolite maintain an optimal level through perturbations by nutrient intake and expenditure. To reach this level of regulation, paracrine and ultimately endocrine regulatory mechanisms had to develop. Paracrine regulation must have been present even at the level single cell organisms and must have been sufficient for multicellular organisms only consisting of a few cells. With increasing size and complexity of the organism, the need for endocrine regulation and a circulatory system arose.

Endocrine regulation allowed for powerful and specific signal transduction at long distance through the circulatory system. This system then allowed for organism wide crosstalk and the development of complex functional processes between clusters of specialized cells pertaining to the maintenance and procreation of the organism. Each process of this nature developed specialized cells that specifically secrete endocrine mediators that modulate it. Conceptually, these cells take in a range of relevant metabolic, paracrine and endocrine parameters and compare them to an internal “homeostatic setpoint”. This homeostatic setpoint determines the homeostatic range that the cell will try to reach by secreting its endocrine products, for example the blood glucose range above which beta cells will start secreting insulin to lower the blood glucose.
The setpoint is individually determined by every secretory cell, combined with paracrine effects, leading to a “wisdom of the crowd” effect. The summation of all these individual responses amount to unimaginable precision and robustness in dosing the response.

The circulatory system also allowed for the rapid transport of nutrients. This led to certain prominent metabolites, that often lie at the intersection of multiple pathways to be used as “currency” within the organism. When judging by relative concentrations and their biochemical structure 5 classes/compounds become apparent: glucose, glutamine, triglycerides, cholesterol and ketones.

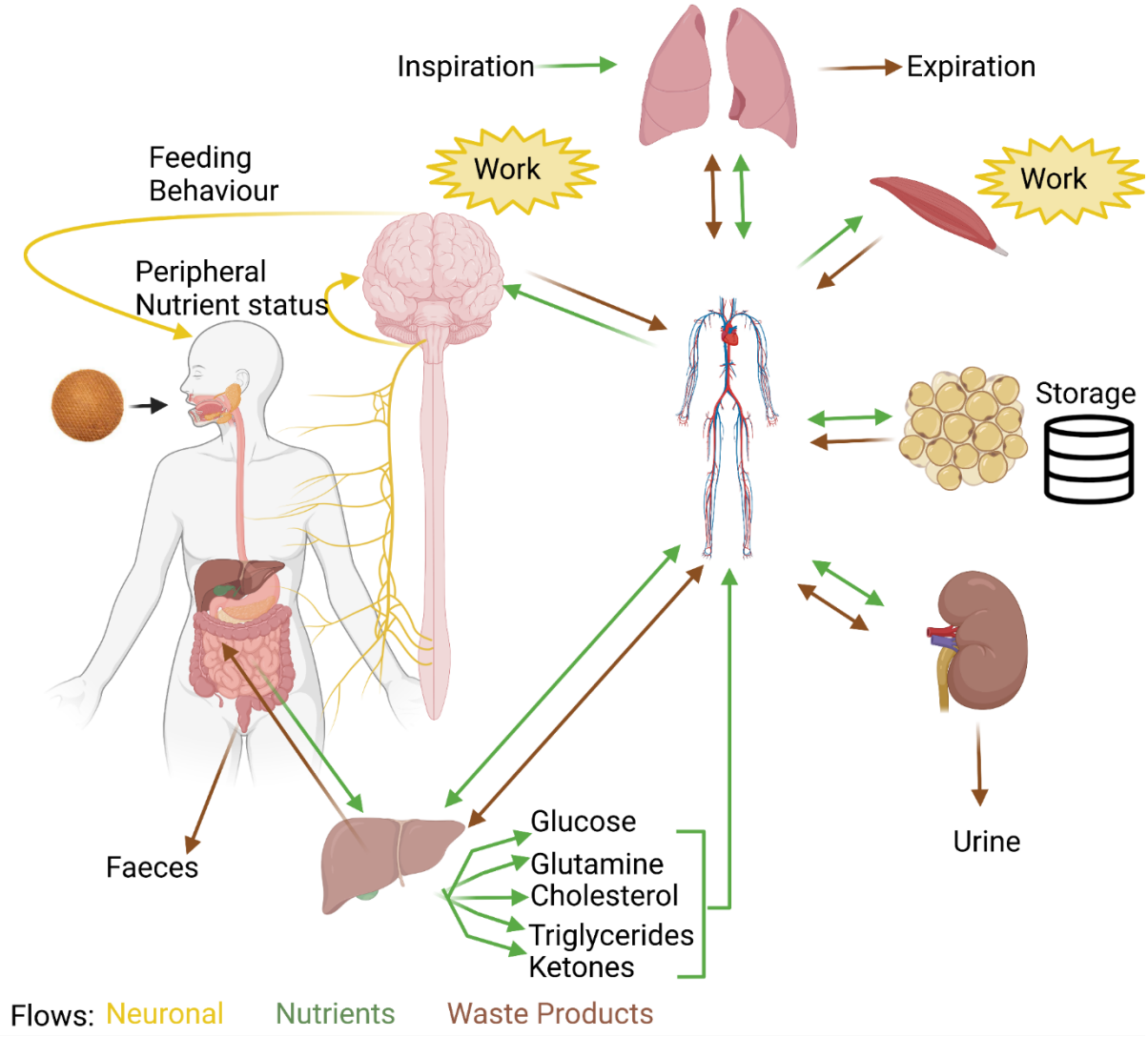


Figure 2 Overview of Mammalian metabolism by first principles. The autonomous nervous system senses the nutritional status of the organism, these inputs are then aggregated in the hypothalamus and relayed to the cortex to induce feeding behaviour. This drives the organism to seek out food and consume the "stroopwafel". The food bolus is then mixed with secretions that promote digestion and the digested metabolites are transported mostly through the portal system. The liver can detoxify and exchange the metabolites to fit the current needs of the organism. The liver then releases the metabolites into the circulation where they are delivered to all the tissues where they consume metabolites to fulfil their function. This results in the production of waste products that can be transported through the circulation and expelled through the breath, sweat, urine and faeces.

## 4.11 Mammalian metabolic system by primary functions

The mammalian metabolic system, in a simplified manner, can be subdivided by its primary functions when going through the process of food consumption.

Starting with feeding behaviour, the hypothalamus integrates peripheral and central inputs regarding nutritional status of the organism[44]. When a certain nutritional threshold is reached, the hypothalamus relays to the cortical regions that food seeking behaviour needs to be initiated. The cortical regions will then combine these inputs with cognitive information to seek out and ingest food[45].

The food bolus is first mechanically broken down in the mouth and mixed with saliva to moisten the food and increase the surface area for chemical and enzymatic digestion. Saliva additionally contains digestive enzymes called amylases that break down polysaccharides[46]. The bolus then travels down the oesophagus to the stomach, containing a highly acidic fluidic that destroys many potential pathogens and further digests the food. The stomach then gradually releases its contents into the intestinal tract where the acidity of the mixture will be neutralized by bicarbonate released by the pancreas together with a range of digestive enzymes[47], breakdown products from the liver and bile from the gallbladder to aid digestion by emulsifying fats. This process progressively digests the nutrients to a state where they can pass through the intestinal barrier.

The small intestine is estimated to be responsible for 90% of the nutrient uptake in the intestinal tract[48]. This is facilitated by the cone shaped intestinal villi that coat the inside of the intestine, drastically increasing its surface area. The villi progressively flatten out towards the large intestine, making it much less permeable. Additionally, the large intestine possesses a thick mucus layer protecting the epithelium. This mucus layer is necessary because the colon houses the majority of the gastrointestinal microbiome[49].

The microbiome is an ecosystem of microorganisms in the gut that digest the remaining nutrients and have formed a symbiotic relationship with their host, competing against foreign, potentially pathogenic, colonizers. The microbiome modulates its host through the products of their metabolism and the host immune system. Since a germ-free gut is impossible outside of animals facilities, the host immune system has to make a compromise to tolerates some bacteria and actively kills others, curating its own microbiome. Disruption of the highly curated microbiome, by for example food contaminants, antibiotics or auto-immune disease, can lead to organism wide dysfunction[50,51].

The majority of the absorbed nutrients from the intestinal tract end up in the portal vein, leading to the liver. As it is the first organ exposed to whatever is absorbed during digestion, the liver serves as a detoxifier. Liver cells express a range of enzymes that catabolize toxic compounds both native and foreign and then release them to the lower digestive tract or circulation. The liver also has the ability to exchange the molecules that lie at the intersection of metabolic pathways such as glucose, glutamine, cholesterol, triglycerides and ketones. Hydrophobic cholesterol and triglycerides are packaged into lipid particles and made soluble by lipoproteins.

Glucose, glutamine and triglycerides represent the three dietary macronutrients: carbohydrates, protein and fat. Ketones are constitutively produced at low levels from fatty acids, but upon nutrient restriction or low carbohydrate consumption, production is ramped up. Ketones are mainly utilized by muscles and neurons, both large consumers of glucose. This suggests that ketones are used as an additional fuel source when the liver is not able the supply glucose demand through gluconeogenesis[52].
Cholesterol composes about 30% of all animal cell membranes, additionally it is used as pre-cursor for the synthesis of steroid hormones, bile acid and vitamin D.
The liver also has storage capacity but this should be considered short-term storage, as accumulation of lipids leads to dysfunction and fatty liver disease[53]. The adipose tissue functions as dedicated long-term storage where reactive, energy rich, molecules are stored as relatively inert triglycerides.

Metabolites are consumed from the circulation for growth, renewal and function. During this process, waste products such as urea, $CO_2$ and lactate are produced and released into the circulation. Hydrophobic waste is handled by the liver whereas hydrophilic waste is handled by the kidneys. The kidneys additionally resorb and limit the amount of water and non-waste products that get released into the urine. This is why glucosuria, indicating blood glucose levels exceeding the kidney's resorptive capacity, has been used to diagnose diabetes as early as the ancient Egyptians[54]. Gaseous waste gets expelled through exhalation, waste processed by the kidneys leaves through the urine and the liver releases its waste into the duodenum. Contrary to popular belief, the skin does not significantly contribute to the disposal of waste products, the process of sweating is primarily for thermoregulatory purposes[55,56].

## 4.12 Metabolic disease

The increase in food productivity by the agricultural revolution has led to a food surplus[57]. This means that for the first time in evolutionary history, humanity has created an environment for itself where food is cheap, abundant, appetizing and nutrient-dense. Given the short time-period in which this change has occurred, not all human individuals have received an adaptive set of genes for these novel conditions. This has caused some individuals to present combinations of excessive feeding stimuli, propensity for storage of energy in the form of fat and an inability to compensate for metabolic stress that ultimately leads to metabolic disease[58].

During an energy surplus through excessive food intake, mechanisms have evolved to conserve excess energy for times when food would be less abundant. During constant food abundance however, these storage mechanisms could be improperly calibrated leading to accumulation of energy resulting in obesity. One could imagine that during this initial stage, small inefficiencies in the disposal of metabolites, leading to small postprandial spikes in extracellular nutrient levels, serve as trophic factors to increase the capacity of the metabolic system leading to adaptations such as: increased islet, liver and adipose tissue mass. During this time, the body is still able to handle the increased demand of storage and overall metabolic parameters will stay within adequate ranges, this state is commonly referred to as "prediabetes"[59].

Behind the scenes, the metabolic system is already being slowly stretched to its limits. For every individual there is a range of metabolic stress that can be accommodated. This limit and the points in the metabolic system that are most prone to failure are determined by genetics and environment and are highly specific to the individual. When this limit is reached, the metabolic system will no longer be able to adequately dispose of postprandial nutrients being introduced into the system through feeding. These undisposed metabolites then disrupt the delicate metabolic balances, creating unwanted reactions, interfering with vital processes. On an organismal level, this leads to the many pathologies that are associated with metabolic disease such as: neuropathy, kidney disease and damage to microvasvulature[60].

## 4.13 Immune system in tissue homeostasis

Through evolutionary processes, receptors for certain pathogens became hardcoded into the genome. Multicellularity further allowed organisms to develop specialized immune cells by co-opting these receptors and combining them with specialized functional response that can be activated upon receptor activation[61]. These cells were specialized in

maintaining the organism's barriers and respond to invading pathogens.
Further tissue-specialization required the same anti-pathogen pathways and cells to be co-opted for facilitating tissue modifications such as matrix remodelling and vascularization to maintain homeostasis[62]. Metabolic stress induces the production of inflammatory cytokines such as IL-1b, TNF-a, and the chemokines CCL2 and LeukotrieneB4. These products are meant to attract macrophages and other immune cells present in the tissue that will drive an inflammatory process to restore tissue homeostasis[63]. When the local immune cells fail to restore homeostasis, cyto- and chemokine levels keep increasing to a point where they start attracting immune cells from the circulation that tend to be drastic pro-inflammatory compared to resident immune cells.

## 4.14 Adipose tissue macrophages

The accumulation of macrophages in the adipose tissue is a broadly described phenomenon in obesity. Hypoxia is hypothesized to be a major driver in adipose tissue inflammation. Adipocytes upregulate ANT2, an ATP/ADP exchanger, to provide more ADP for TCA-cycle based lipolysis in response to high levels of free fatty acids associated with obesity. This increased TCA-cycle flux also consumes significant $O_2$ that needs to be provided by the circulation, as exemplified by lower levels of $O_2$ measured in obese adipose tissue[64].
Adipocyte specific deletion of the hypoxia responsive transcription factor Hif-1a has been shown to prevent the development of adipose tissue inflammation and macrophage infiltration, suggesting adipose tissue hypoxia as a driver of adipose tissue inflammation[65]. During normoxia, Hif-1a is constantly hydroxylated by prolyl hydroxylase domain proteins (PHDs) which directs it towards proteasomal degradation. During hypoxia, PHDs are inactivated and Hif1a is stabilized, activating a transcriptional program that responds to hypoxia with metabolic adaptations and the secretion of chemokines[66]. Accumulation of succinate can also inhibit PHDs, leading to Hif1-a stabilization and the production of cytokines and chemokines[67].
This results in the accumulation of so-called "Lipid associated macrophages" that are largely derived from monocytes and aggregate in "crown like structures" around adipocytes[68]. The expansion of these macrophages is mediated by Trem2. Therefore deletion of *Trem2* leads to increased metabolic dysfunction, underlining the importance of macrophages maintaining tissue homeostasis.

## 4.15 Insulin and glucose disposal

Glucose is the starting point for glycolysis and the PPP. Pyruvate, the end-product of glycolysis, can either be fermented into lactic acid or, when oxygen levels are accommodating, enter the TCA cycle in the mitochondria. Glucose can be cytotoxic in high concentrations through over-feeding glycolysis and the downstream ROS-producing pathways or the formation of glycation products by reacting with amines in the Maillard reaction[69]. Many immune cells express RAGE receptors, that recognize advanced glycation end products and activate a pro-inflammatory program to restore homeostasis and prevent further production of these RAGE ligands[70]. Glucose homeostasis is therefore tightly regulated by, among other factors, the peptide hormone insulin.
When insulin binds the insulin receptor (IR), its tyrosine kinase is activated. This causes tyrosine phosphorylation of IR and the IR substrate (IRS) proteins. Phosphotyrosine sites on IRS allow binding of the lipid kinase PI3K, which converts components of the plasma membrane to the signalling molecule PIP3. This recruits the phosphoinositide-dependent kinase (PDK), which directly phosphorylates AKT. Activated AKT phosphorylates a number

of substrates at Ser/Thr residues. Targets of AKT include: the forkhead family box O (FOXO) transcription factors, the protein tuberous sclerosis 2 (TSC2), glycogen synthase kinase 3β (GSK3) and the RabGAP TBC1 domain family member 4[71] (TBC1D4). Insulin signals tissues to take up glucose from the environment where possible by, for example, translocation of Glut4 glucose channels to the plasma membrane[72]. Additionally, insulin signals to the liver that it should reduce its gluconeogenesis since there is enough glucose in the circulation. The immune cells recruited by cells experiencing metabolic stress produce cytokines that induce insulin resistance. Insulin resistance is characterized by lack of responsiveness to insulin, it can be induced by cytokines or intrinsically developed by cells no longer being able to take in more nutrients as a safety mechanism to prevent metabolic induced cellular dysfunction. Macrophage derived TNF-a can induce inhibitory phosphorylation of IRS and lower the expression of *Irs2* and *Glut4* , which is a glucose transporter expressed on adipocyte.
When the body is no longer able to produce adequate amounts of insulin to sequester the glucose from the circulation, hyperglycaemia occurs which is one of the hallmarks of diabetes. Type 2 diabetes (T2D) is characterized by insulin resistance, often as a result of obesity[73]. T2D at first presents as hyperinsulinemia with possibly mild hyperglycaemia and, when no significant life-style changes are made, later decompensates with insulin levels dropping off accompanied by overt hyperglycaemia and the need for exogenous insulin[74].

## 4.15 Metabolic regulation of insulin secretion

Insulin is rapidly secreted by specialized cells called beta cells in response to elevations in glucose concentration in the circulation. Beta cells have specialized their physiology in order to detect glucose concentrations with high precision. The beta cell surface has a high density of glucose transporters which causes intracellular glucose concentrations to quickly equilibrate between the cytoplasm and the extracellular space[75]. Beta cells also express glucokinase, an alternative hexokinase that, unlike other hexokinases, is not subject to allosteric inhibition[76].Once the glucose concentration reaches above a threshold value of ~5mM,  it is converted immediately, regardless of possible congestion of downstream pathways. This unrestricted flux of glucose metabolism makes beta cells especially sensitive to redox stress induced by hyperglycaemia. This causes the product, glucose-6-phosphate, which stands at the crossroad of glycolysis and PPP to flow maximally into both pathways.  Insulin secretion is then coupled to the many (by-)products of glucose catabolism and oxPhos, ranging from ATP and glutamate to ROS[77], ultimately resulting in membrane depolarization.

## 4.16 Mechanism of insulin secretion

Insulin is initially produced as pre-proinsulin. Through co-translational insertion, the signal peptide (24 amino acid residues from the N-terminus of the protein) is cleaved and the resulting proinsulin is delivered to the Golgi apparatus. Proinsulin consists of three domains: the B chain at the N-terminus, the A chain at the C-terminus and a connecting middle peptide termed C peptide. During maturation, proinsulin is exposed to several specific endopeptidases which excise the C peptide, thereby generating the mature form of insulin. Insulin is crystalized and packaged into secretory granules at the trans-Golgi network, together with ATP, C-peptides, GABA and glutamate. Mature vesicles migrate to the plasma membrane, with the aid of motor proteins. In response to high glucose concentration, membrane polarization occurs through the aforementioned metabolic mechanisms, resulting in vesicle exocytosis.

## 4.17 Pancreatic islets

Beta cells are located in the pancreatic islets of Langerhans that are interspersed as "islands in a sea" of exocrine pancreatic tissue. Islets are clusters of cells consisting of glucagon producing alpha cells, insulin producing beta cells, somatostatin producing delta cells, ghrelin producing epsilon cells, pancreatic polypeptide producing gamma cells, epithelial cells and immune cells (mostly macrophages)[78,79]. In mice, beta cells comprise ~90% of the cells in islets regardless of their size. In humans, the percentage of beta cells seems to decrease with larger islets down to 50% in the largest islets, additionally larger islets also tend to be less abundant in humans with T2D. The islets are more perfused than the exocrine pancreas, receiving 10-15% of the blood flow while comprising only 1-2% of total organ mass[80,81]. Together with the GI-tract, islets release a well-measured combination of metabolic hormones for proper disposal of the post-prandial increase in blood metabolites.

## 4.18 Islet Macrophages

Depending on their size, islets on average contain ~10 macrophages[79]. Macrophages perform various functions within the islets such as scavenging apoptotic cells[82], clearing bacterial components[83] and acutely signalling insulin secretion through IL-1b release[84]. Islet macrophages have also been implicated as mediators of islet inflammation and islet dysfunction[85]. Contrary to the adipose tissue and liver, islets rely on local proliferation of islet macrophages rather than recruitment of monocyte derived macrophages[86]. Recruited monocytes are only detected in the peri-islet area.

In response to increased insulin demand and beta cell death, Islet macrophage produce factors such as PDGF and IGF-1 to promote islet proliferation[87].

There are two distinct macrophage types in the islet environment: intra- and peri-islet macrophages[86]. The intra-islet macrophage population itself also has a high degree of heterogeneity as shown by recent single cell transcriptomic datasets (unpublished).

Only intra-islet macrophages drastically proliferate during obesity, while peri-islet macrophages do not. Additionally, only intra-islet macrophages have been shown inhibit insulin secretion[88]. This is likely mediated through contact dependent effects, phagocytosis of insulin granules and chronic secretion of pro-inflammatory cytokines. Chronic IL-1b signalling for example induces NF-κB and JNK signalling resulting in nitric oxide production by inducible nitric oxide synthase[89]. This nitric oxide can oxidize ISCs of ETC and oxPhos enzymes, thereby inactivating them. This will diminish the activity of these pathways, resulting in less product formation that metabolically stimulates insulin secretion.

## 4.19 Macrophage activation and System Xc-

When macrophages are activated by TLR4 ligands such as lipopolysaccharides (LPS), profound metabolic, transcriptomic and epigenetic changes within the cell drive an anabolic response. Macrophages become more insulin sensitive and start taking up and utilising more glucose by increasing the flows into glycolysis and PPP[90].

Upon activation, macrophages form breaking points in their mitochondrial metabolism, leading to accumulation of citrate and succinate. The accumulated citrate can be exported to the cytosol, where it is degraded by ACL back to acetyl-CoA and oxaloacetate, which itself can be converted to acetyl-CoA. The increase in acetyl-CoA can then be used to induce histone acetylation, epigenetically cementing the inflammatory program[91]. Acetyl-CoA can also be used to synthesize malonyl-CoA, that serves as a precursor for fatty acids

and cholesterol, used for the production of lipid rafts and prostaglandins[92]. Malonyl-CoA synergistically functions in a feedback loop inhibiting CPT1, thereby preventing fatty acid translocation from the cytosol to the mitochondria. Moreover, malonyl-CoA has the capacity to malonylate lysine residues of proteins, which is a post-translational modification associated with inflammation that is enriched in mouse models of T2D[93]. Indeed, malonylation of GAPDH has been shown to promote TNF-a production in macrophages, by dissociating *Tnfa* mRNA from GAPDH and promoting its translation[94]. Cis-aconitate from Citrate can also be converted to itaconate, an anti-bacterial compound with anti-inflammatory properties[95]. Itaconate can inhibit complex II of the ETC, further contributing to the accumulation succinate. Additionally, itaconate can be transported to the cytosol, where it activates the transcription factors Nrf2 and Atf3 that inhibit IL-1b and IL-6 transcription respectively.
When activated, macrophages also accumulate succinate intracellularly. This build-up prevents the breakdown of Hif1-a by PHDs which activates an inflammatory program sharing overlap with the response to hypoxia[67]. Additionally, macrophages start secreting succinate and simultaneously upregulate the succinate receptor (SUCNR1). SUCNR1 is G-protein coupled receptor that promotes IL-1b production in macrophages, thereby further increasing succinate production in a feedback loop[96].
Mitochondria have the capability to produce vast amounts of ROS through the ETC, macrophages have harnessed this as a weapon to combat pathogens with respiratory bursts. This phenomenon is triggered by obstruction and reversal of the ETC, leading to the donation of electrons to oxygen, generating superoxide. This process is driven by lower or reverse TCA cycle flux, hypoxia and succinate accumulation[97].
Part of the downstream response to LPS is a rapid (within 1 hour) upregulation of *Slc7a11*, the light chain of sXc, in order to supply enough cysteine for the anabolic response and mitigate the increased ROS production. Although the exact transcriptomic mechanism is not known, it is likely to be a combination of Hif1-a, Atf4 and Nrf2, depending on the environment and cellular state[98]. In models of brain ischemia re-perfusion and endotoxemia, the glutamate export activity of sXc by glial cells has been described as an important driver of a specific type of neuronal cell-death termed excitotoxicity that is characterized by excessive glutamatergic signalling[99,100].

## 4.20 Beta cells and excitotoxicity

Beta cells share much with neurons in terms of transcription factors, membrane potential fluctuations and evolutionary origins[101]. Indeed, glutamate sensitive NMDA receptors modulate insulin secretion[102]. Additionally, pharmacological inhibition of NMDA receptors with memantine has been shown the reduce the inflammation and severity of diabetes[103]. We therefore hypothesized excitotoxicity might also be occurring in beta cells in the context of obesity. Given the high sensitivity of beta cells to redox stress and the possible occurrence of excitotoxicity, we studied whole body *Slc7a11* -/- mice and generated conditional myeloid-specific *Slc7a11* knockouts. Lack of *Slc7a11* leads to drastically lowered glutathione levels in the pancreatic islets and defective insulin secretion both *in vitro* and *in vivo*. We also observe a compensatory increase in insulin sensitivity that is abrogated upon dietary challenge. We did not find any evidence of excitotoxicity or islet dysfunction in myeloid specific knockout animals. *In vitro* we did find defective cytokine production in *Slc7a11* deficient macrophages and. We also observed altered mitochondrial function, suggesting reduced mitochondrial flexibility. Our findings outline an important role for cysteine and glutathione and thereby sXc in beta cell biology and macrophage function, but

do not support sXc mediated excitotoxicity playing a major role in obesity induced islet dysfunction.

# 5. Results

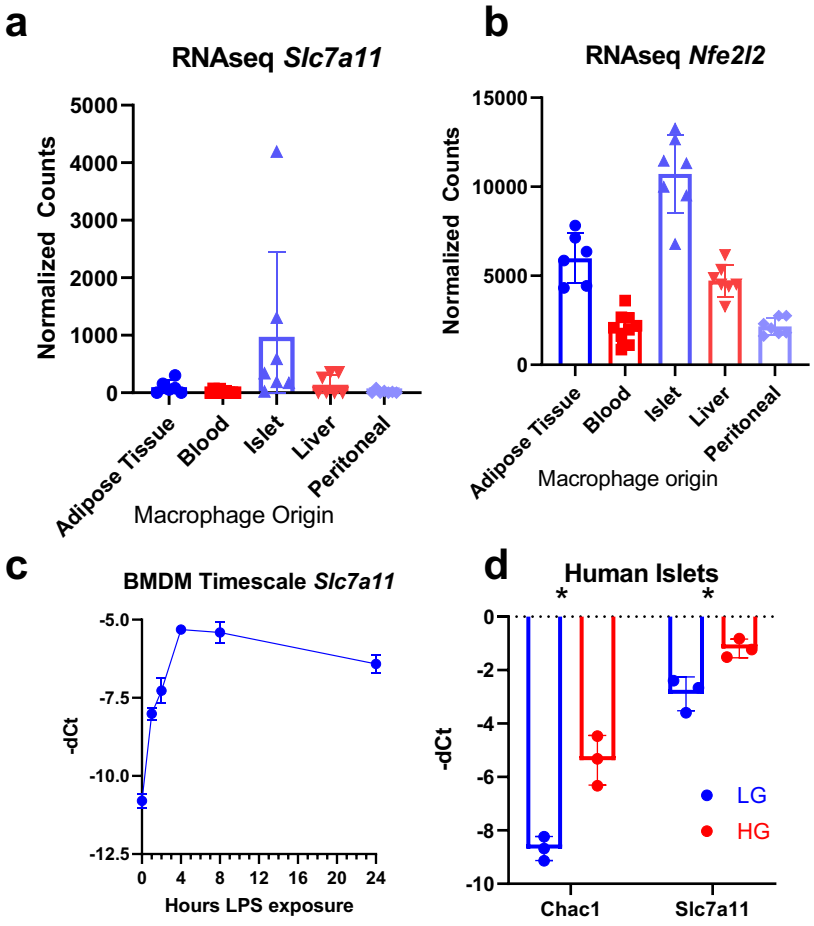


Figure 3 Expression pattern of Scl7a11 and associated genes. a,b RNAseq data of different macrophage subtypes c, timescale rtPCR for Slc7a11 LPS exposure of BMDM timesline (d) rtPCR of Human islets exposed to 22.2mM (HG) compared to 5.5 mM (LG) glucose for 3 days. Statistics: Student's t test; error bars represent SD; $^{\star}p < 0.05$.

## 5.1 Observational data

Because the implication of sXc in excitotoxicity and existing evidence supporting excitotoxicity in beta cells we decided to investigate sXc in the context of insulin secretion. Initially we did some preliminary experiments to see what macrophage subtypes express the sXc lightchain *Slc7a11*. We also consulted a previously generated bulk RNA-seq dataset[104]. We found that between adipose tissue, blood, liver, islet and peritoneal macrophages (PMs), *Slc7a11* was highest expressed in islet macrophages (fig 3a). Additionally, we found Nfl2e2, encoding the redox regulatory transcription factor Nrf2, which is promotes *Slc7a11* expression, to be preferentially expressed in islet macrophages (fig 3b). We have also observed that *Slc7a11* is rapidly upregulated in wild-type bone marrow-derived macrophages (BMDMs) exposed to 100 ng/mL LPS (fig 3c). An upregulation of *Slc7a11* and *Chac1*, encoding a glutathione degrading enzyme that is activated upon cysteine shortage within the cell, was observed in human islets after 3 days of incubation at 22.2mM glucose (fig 3d).

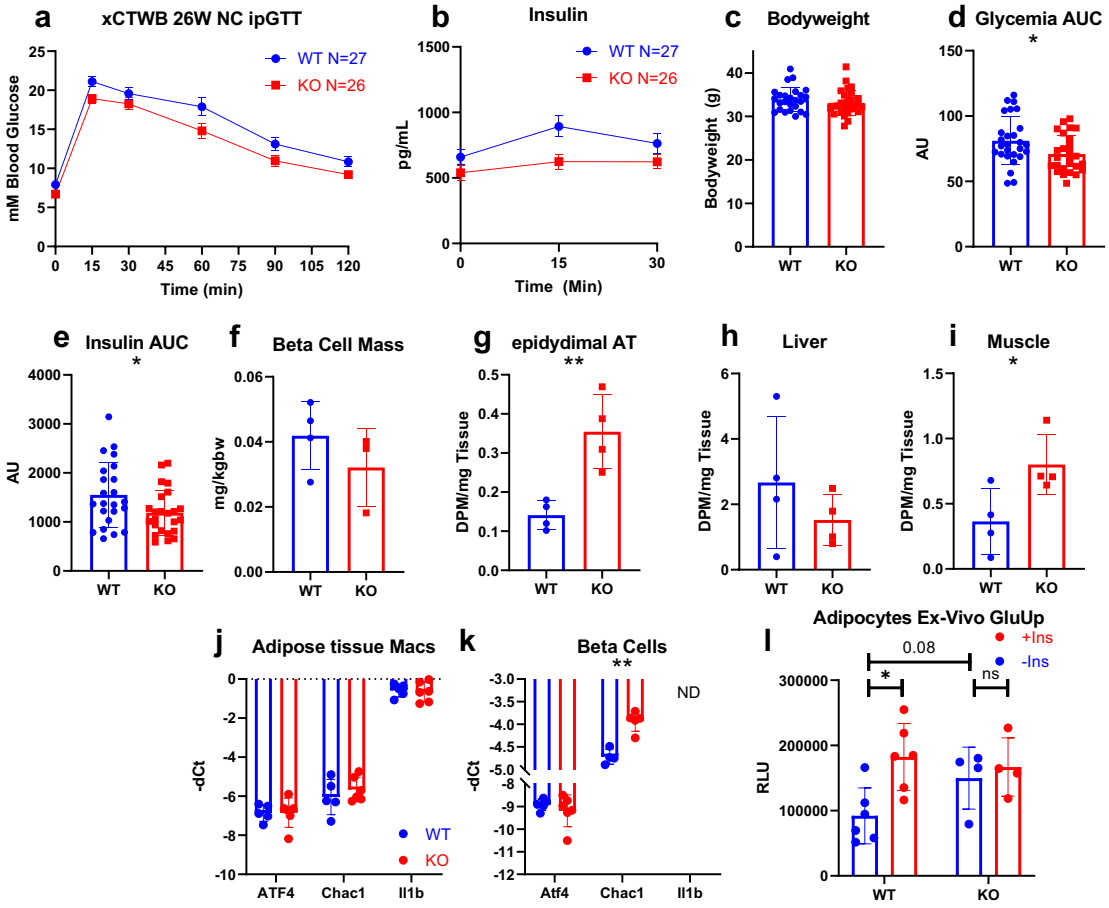


Figure 4 Metabolic phenotype of xCT knockout mice at 26 weeks. (a) ipGTT glycemia, (b) Insulin, (c) Bodyweight, (d) AUC of glycemia, (e) AUC of insulin, (f) beta cell mass normalized to pancreas weight/bodyweight (g-i) beta cell mass, [3H]2-deoxyglucose uptake in Epididymal Adipose Tissue, liver (h) and muscle (j,k) rtPCR of sorted ATMs and beta cells, (l) glucose uptake in isolated adipocytes. Statistics: Student's t test; (a,b) error bars represent SEM, (c-k) error bars represent SD; *p < 0.05, **p < 0.01.

## 5.2 Slc7a11-/- mice have reduced insulin secretion and increased glucose disposal in later life

In order to further understand the role of sXc in the context of metabolism, whole body knockouts with a disrupting GFP cassette cloned into the *Slc7a11* gene region were acquired and metabolically phenotyped. At 26 weeks of age, the animals started showing increased disposal of glucose in response to a glucose bolus in an intraperitoneal Glucose Tolerance Test (ipGTT) (fig 4a). Additionally they showed a reduced secretion of insulin in response to the glucose bolus while not having a different bodyweight at this age (fig 4b,c). Both insulin and glycemia reached statistical significance for the area under the curve (AUC) (fig 4d,e). To investigate whether this diminished insulin secretion is a result of reduced beta-cell mass, histological analysis was performed to determine the ratio of islet area to exocrine area that was then multiplied by pancreas weight normalised to bodyweight (fig 4f). We did not find a statistical difference in beta cell mass between the groups, indicating the animals were able to maintain their beta cell mass. We then found increased tritium labelled 2-deoxyglucose uptake in the epididymal adipose tissue (eAT), liver and muscle in an ipGTT setup, sacrificed 30 minutes post injection. There was no difference found in liver and significantly higher glucose uptake in muscle (fig 4h,i). To further investigate the cause of the increased glucose uptake in eAT, we isolated RNA from ATMs (ATMs) and performed

rtPCR for *Atf4* and *Chac1*, both genes associated with cysteine shortage, in addition to *Il1b*, a pro-inflammatory cytokine associated with metabolic disease (fig 4j). We did not find a difference in the expression of these genes in ATMs but we found an upregulation of *Chac1* in side-scatter-based sorted beta cell-enriched fraction of pancreatic islets (fig 4k). Finally, we assessed glucose uptake in isolated adipocytes (fig 4l). We found a lack of response to insulin in xCT knockout adipocytes with a trend towards higher basal glucose uptake, matching our *in vivo* data (fig 4l).

## 5.3 Pre-treatment with LPS stimulates insulin secretion

Since sXc is rapidly upregulated upon LPS stimulation, we investigated the effect of pre-injection with 2mg/kgbw LPS for 6 hours before the experiment in 26-week-old whole-body xCT KO animals. LPS pre-treatment greatly increased insulin secretion and glucose disposal, to an extent where the observed phenotype observed without LPS treatment was no longer visible (fig 5a-c). Additionally, we assessed plasma IL-1b levels 6 hours post injection and did not find a difference between the groups (fig 5d). We also assessed whole blood GSH levels in WT and KO animals along the track of LPS treatment, despite the reported difference in serum GSH levels[105] (fig 5e), we could not measure a statistically significant difference between the groups in whole blood.

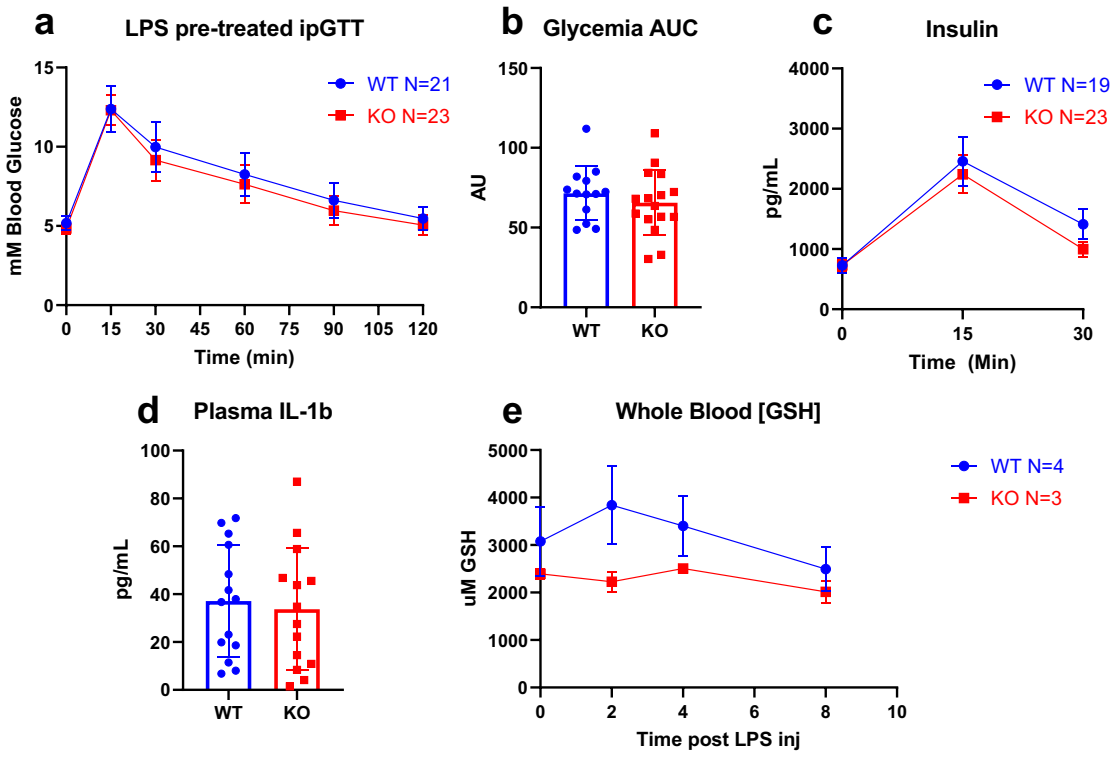


Figure 5 ipGTT with LPS pre-treatment 26W WholeBody KOs, (a-c) ipGTT with LPS pre-treatment, (d) plasma IL-1b levels 6 hours post 2mg/kgbw LPS injection, (e) whole blood GSH timescourse, (a,c,e) error bars represent SEM, (b,d) error bars represent SD.

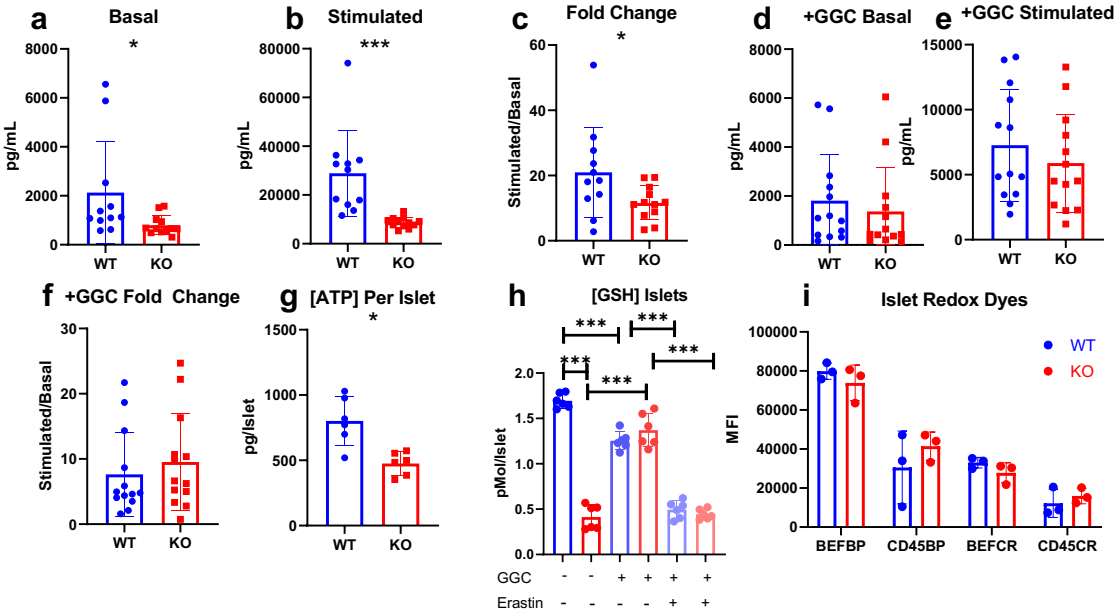


Figure 6 Functional aspects of isolated islets (a-c) Glucose stimulated insulin secretion, (d-f) GSIS of islets treated with 1mM γ-glutamyl-cysteine for 24 hours, (g) ATP levels per islet, (h) Glutathione concentration per islet, (i) ROS and Lipid peroxidation with Cellrox(CR) and Bodipy C11 (BP). Statistics: Student's t test; error bars represent SD; *p < 0.05, ***p < 0.001. (a-f) Each dot represents a pooled sample of 5 islets 3 mice used per group, (g,h) each dot represents a 10 islet sample from 1 mouse, (i) each dot represents one mouse.

## 5.4 SXc is vital for *in vitro* islet glutathione levels and glucose stimulated insulin secretion

To investigate the functional consequences of sXc deficiency on islet function, islets were isolated and assessed in by *in vitro* glucose stimulated insulin secretion (GSIS). This involves measuring insulin secretion at 5.5mM and 16.7mM glucose to determine the insulin response to elevated glucose levels. We found that sXc deficient islets had significantly diminished basal (5.5mM) and stimulated (16.7 mM) insulin secretion. Furthermore, fold change (stimulated/basal) was also significantly decreased (fig 6a-c). We then wondered if supplying glutathione by incubation with 1mM γ-glutamyl-cysteine (GGC), a pre-cursor of glutathione (GSH), for 24hours could rescue the impaired secretory phenotype. Although it eliminated the difference between the groups, it also significantly reduced the amount of insulin secreted in general and fold change of the WT islets. This effect was not observed in the sXc KOs (fig 6d-f).

ATP levels in size-matched KO islets were assessed. We found a reduction in ATP levels, suggesting either a reduced mitochondrial activity or cell viability (fig 6g). We then determined GSH levels in whole islets and found lower GSH in knockout islets (fig 6h). This reduction could be partially rescued with 24h GGC treatment. Interestingly, GGC treatment brought down the GSH levels of WT islets to the level of KOs. An additional group of islets was treated with 5uM Erastin, a widely used inhibitor of sXc, in addition to GGC for 24 hours. Despite lacking the transporter, Erastin treatment drastically lowered the GSH levels in KO islets treated with GGC. Our findings therefore underline the sXc-independent effects of Erastin on cellular GSH levels. Given the lower levels of GSH, we investigated reactive oxygen species (ROS) and lipid peroxidation (fig 6i). Surprisingly, there was no difference between WT and KO islet fractions, suggesting the lower glutathione levels are still adequate for maintaining redox homeostasis.

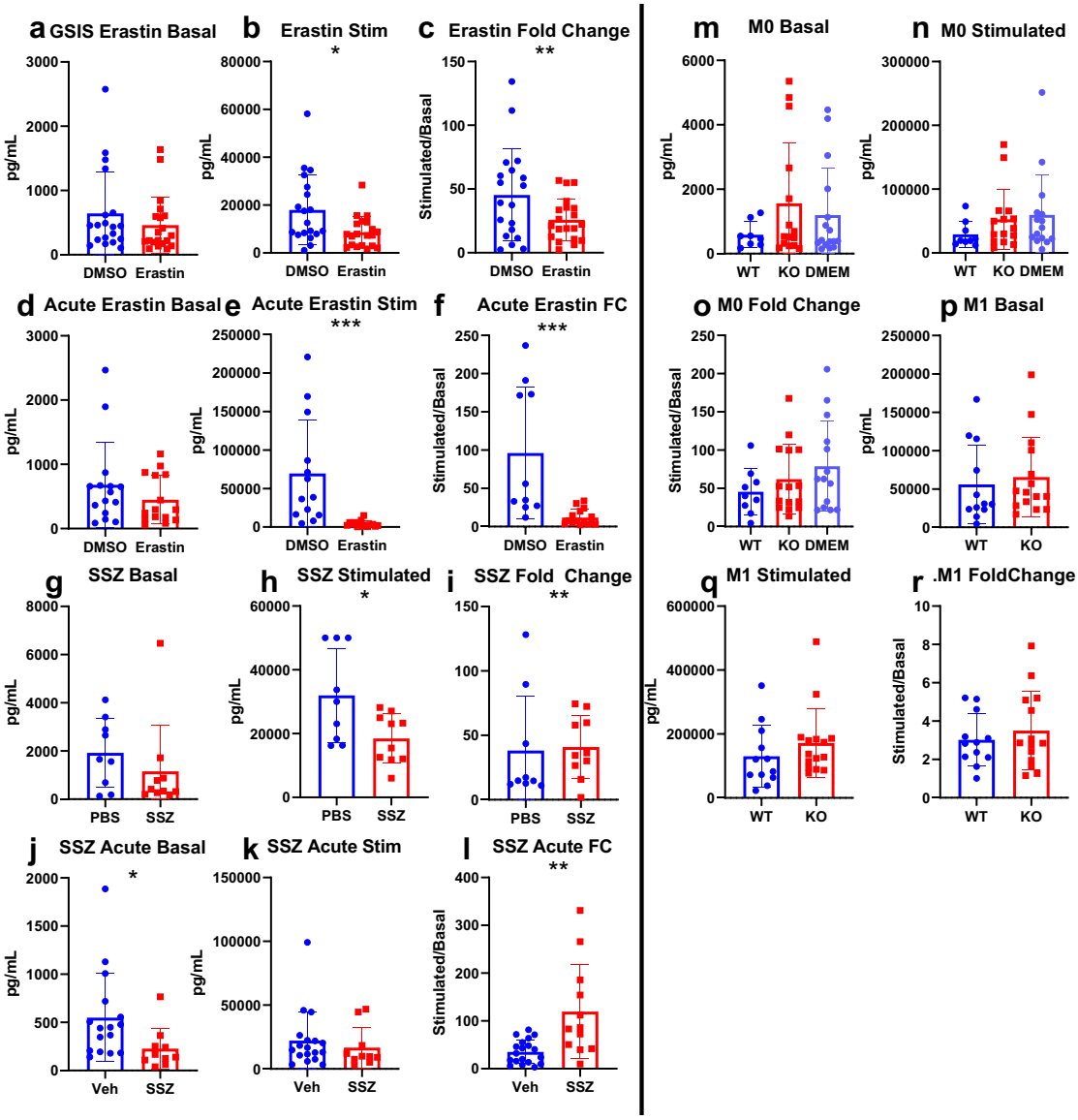


Figure 7 Effect of sXc inhibitors on insulin secretion and co-culture experiments (a-c) GSIS of islets treated with 5uM Erastin for 24 hours, (d-f) GSIS of islets exposed to 5uM Erastin in the high glucose (stimulated) medium, (g-i) GSIS of islets exposed to 0.1mM Sulfasalazine (SSZ) for 24 hours, (j-k) GSIS of islets exposed to 0.1mM SSZ in the stimulated medium, (l-n) GSIS islets incubated for 24hours in medium conditioned by M0 macrophages for 24hours, (o-r) GSIS of islets incubated in M1 conditioned medium. Statistics: Student's t test; error bars represent SD; *p < 0.05, **p < 0.01, ***p < 0.001. Each dot represents a pooled sample of 5 islets, 3 mice were used per experiment.

## 5.5 SXc inhibitors have differential effects on GSIS

In order to study the role of sXc in the acute phase of GSIS, we performed GSIS with two pharmacological sXc inhibitors: Sulfasalazine (SSZ) and erastin. Upon 24hour treatment, erastin significantly diminishes stimulated insulin secretion (fig 7a-c). When given in an acute setting, only upon high glucose stimulation, erastin almost completely abolishes insulin secretion (fig 7d-f). Islets treated with sulfasalazine for 24h trends towards lower basal secretion and a significantly lower stimulated secretion. This leads to a significantly higher fold change in insulin secretion but with lower overall secretion(fig 7g-i). When assessing SSZ in the acute setting, there was unfortunately a significantly lower basal secretion between both untreated groups (fig 7j-k). Administration of SSZ upon high

glucose stimulation did therefore not lead to a significant increase in insulin secretion but the insulin potentiating effects of SSZ were reflected in the fold change.
We then sought to find out whether sXc deficient macrophage might be differentially secreting paracrine factors that could affect insulin secretion by islets. We conditioned medium for 24 hours with BMDMs either unpolarised (M0) or polarized with 100ng/mL LPS for 24 hours (M1). We did not find any statistically significant differences in GSIS between the experimental groups in medium conditioned by M0 macrophages (fig 7m-o). In contrast, we found that medium conditioned by M1 macrophages drastically reduced insulin secretion but did not find differences between the genotypes either (fig 7p-r).

## 5.6 SXc is vital for mitochondrial function and cytokine production in BMDMs

Macrophages show rapid upregulation of sXc upon activation by LPS, this suggests a special role for sXc in macrophage function. To this end, we decided to take a more in depth look into macrophage function *in vitro*. We generated bone marrow-derived macrophages from wild-type and sXc knockout animals. We studied macrophages in several polarizations: M0, M1, M2 and Mox, polarized by no treatment, treatment with 100ng/mL LPS, 40ng/mL IL-4 and 50ug/mL oxPAPC, respectively. We first assessed GSH intracellular in the differently polarized macrophages (fig 8a). We found a reductions in GSH across the polarizations between the genotypes. Additionally, M1 polarization led to lower GSH levels in KO BMDMs. Polarization to Mox significantly increased the GSH levels in WT BMDMs and treatment with GGC increased the GSH levels of KO BMDMs but also reduced the GSH levels of WT macrophages to a similar level.
To assess whether the lower intracellular levels lead to lower GSH secretion into the medium, we assessed GSH levels of medium cultured by the same macrophages the intracellular levels were measured of. Lower GSH levels were found for medium cultured by KO compared to WT macrophages, the difference was less pronounced than the differences observed in intracellular GSH.
Interestingly, treatment with GGC increased medium GSH for KO BMDMs but did not reduce WT medium GSH the same way it does for intracellular GSH. M2 polarization also lowered the amount of GSH exported into the medium by WT BMDMs. In addition to GSH, we measured the anti-oxidant potential of the medium and found it to be significantly lowered in polarized macrophages (fig 8c). Additionally, polarization increased the anti-oxidant potential of the medium of WT macrophages.
Thiol levels were then assessed using a thiol reactive dye with subsequent flow cytometry analysis. SXc knockout macrophages had lower Thiol levels (fig 8d) when not polarized or polarized with LPS. Interestingly, treatment with Zymosan (a TLR2 agonist) drastically increases fluorescence in both WT and KO macrophages but did not result in a difference between the groups.
IL-1b secretion was assessed *in vitro* by measuring IL-1b in the supernatant and normalizing it to protein levels as measured by BCA (fig 8e). SXc deficient macrophages had significantly lower IL-1b secretion that could be partially rescued by 24h treatment with 1mM GGC (fig 8e). We also assessed IL-10 secretion and found that KO macrophages produce less IL-10 and this reduction cannot be rescued by GGC treatment (fig 8f).
Since too much GSH could potentially lead to ER stress, we measured *Chop1* expression by rtPCR after 24hour treatment at different GGC concentrations (fig 8g). Unpolarized macrophages did not upregulate *Chop1* even at 5mM concentrations whereas activated macrophages showed a significant upregulation at 1mM and 5mM GGC.
We then assessed *Slc7a11* in different macrophage polarizations and found that sXc is selectively upregulated in M1 macrophages (fig 8h). Despite their redox-related phenotype,

mox macrophages showed no upregulation of *Slc7a11*.
Given the defect in cytokine secretion, we then sought to assess intracellular cytokines by antibody staining and subsequent flow cytometric analysis. Stimulated KO macrophages seemed to have higher levels of intracellular IL-1b, which is paradoxical, given the lower IL-1b secretion (fig 8i). Surprisingly after 1 hour of 2 mM ATP treatment, which is necessary for IL-1b to be released into the medium in the *in vitro* secretion experiment, there was no difference in IL-1b fluorescence intensity.
IL-10 levels were already higher in KO macrophages at baseline, the difference persisted through activation while activation did increased the fluorescence intensity in both WT and KO macrophages (fig 8j). Interestingly, ATP treatment also increased IL-10 fluorescence in macrophages.
We then measured mitochondrial membrane potential by analysis of macrophages stained with two mitochondria reactive dyes: mitotracker green, that stains all mitochondria irrespective of activity, and mitotracker red, that stains mitochondria based on their membrane potential. When plotting mitotracker red versus mitotracker green, two distinct populations could be identified: PE-hi and PE-lo, corresponding to their mitotracker red intensity (fig 8k). Upon LPS treatment the PE-Hi population decreased but this decrease was less pronounced in KO macrophages (fig 8l). When assessing the membrane potential per mitochondrion, we saw that in the PE-lo population, KO macrophages had higher membrane potential and macrophages in the Hi population had lower membrane potential, suggesting mitochondrial inflexibility (fig 8m,n). Mitochondrial superoxide was also assessed using a superoxide reactive flow cytometry dyes. Unstimulated KO macrophages already had higher superoxide levels (fig 8o). When the macrophages are activated with LPS, there is a drop in superoxide fluorescence which does not reach statistical significance in the KO but does in WT macrophages. Treatment with Zymosan further increased superoxide fluorescence in the WT but not KO macrophages.

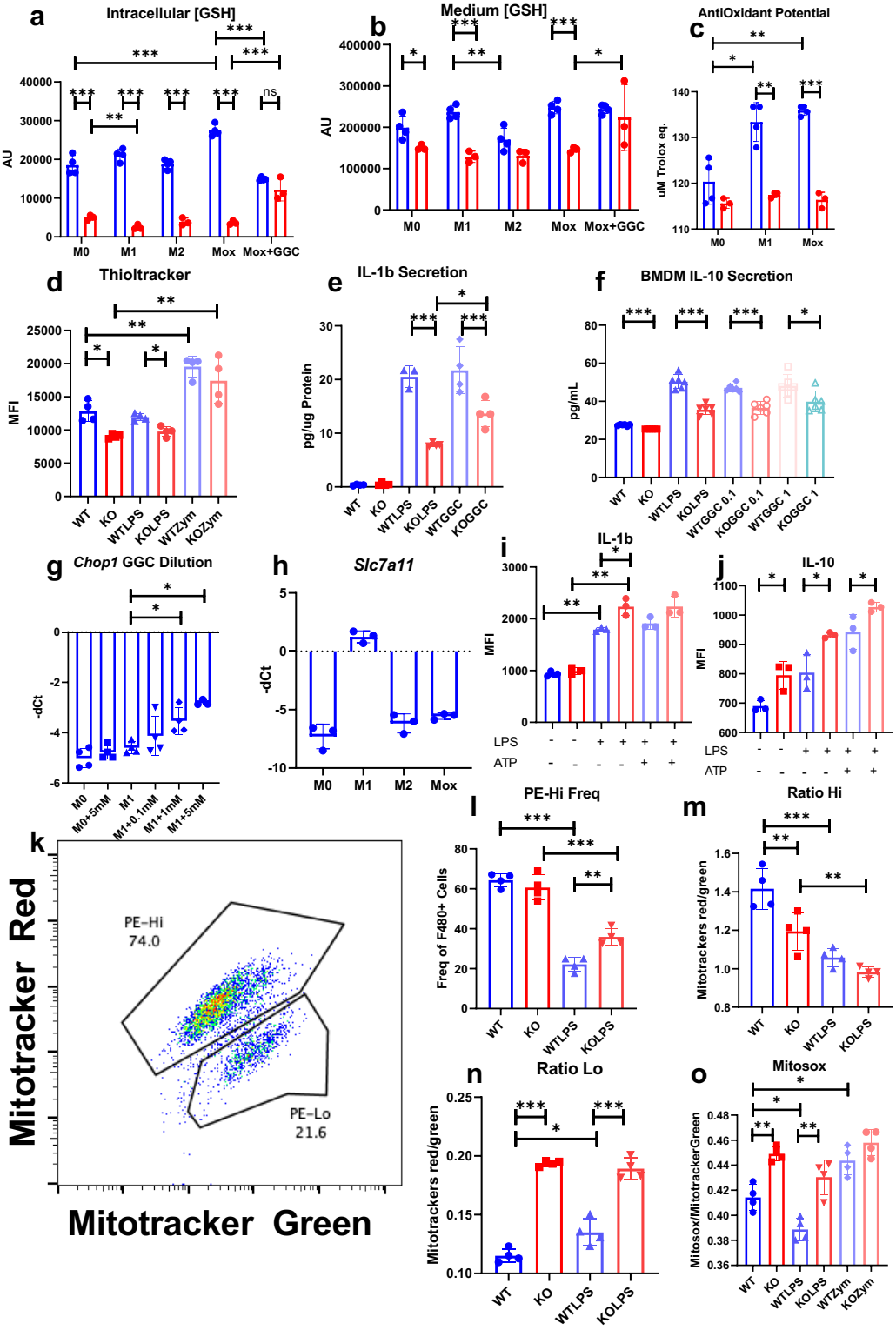


Figure 8 Bone marrow derived macrophages (a) Intracellular glutathione, (b) extracellular glutathione, (c) anti-oxidant potential of medium, (d) Thioltracker thiol determination, (e) In vitro IL-1b secretion, (f) In vitro IL-10 secretion, (g) Chop1 expression in GGC Dilution series, (h) Slc7a11 expression in macrophage polarizations, (i-j) Intracellular cytokine staining, (k) Population plot of mitotracker populations (l-n) Mitotracker population frequency and mitochondrial membrane potential (o) Mitochondrial superoxide detection. Statistics: Student's t test; error bars represent SD; *p < 0.05, **p < 0.01, ***p < 0.001.

## 5.7 Chac1 is necessary for macrophage function

Since *Chac1* is the most consistently upregulated gene we found in sXc deficient cells, we decided to generate *Chac1* knockout BMDMs by electroporation of Cas9 with a *Chac1* guide complex. The knockout lowered *Chac1* expression by ~2 Cts and led to a mild upregulation of ER stress genes *Chop1* and *Xbp1-s* (fig 9a). We then assessed macrophage function through IL-1b secretion and found that disruption of *Chac1* resulted in higher IL-1b secretion in control BMDMs while it further disrupted IL-1b production in KO macrophages (fig 9b). Finally, we assessed GSH levels and found the levels to be lowered in both WT and KO BMDMs electroporated with the guides compared to mock electroporation, when stimulated with LPS. This finding is paradoxical, given the GSH-degrading activity of Chac1 but could be attributed to impaired cellular function (fig 9c).

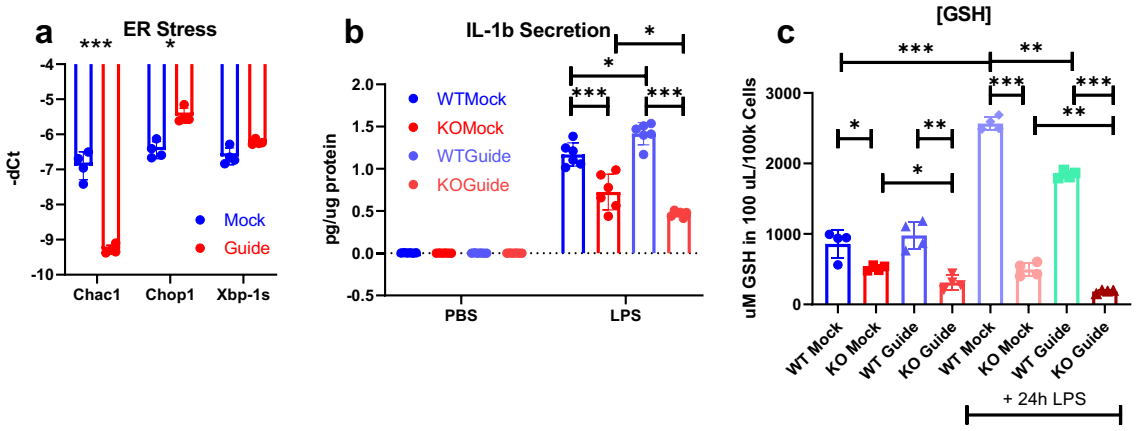


Figure 9 Cas9 disruption of Chac1 in BMDMs, (a) rtPCR of Cas9 electroporated BMDMs, (b) IL-1b secretion, (c) intracellular glutathione levels. Statistics: Student's t test; error bars represent SD; *p < 0.05, **p < 0.01, ***p < 0.001. (a,c) Each dot represents a biological replicate from one batch of electroporated BMDMs (b) Each group contains 3 replicates of 2 separate experiments.

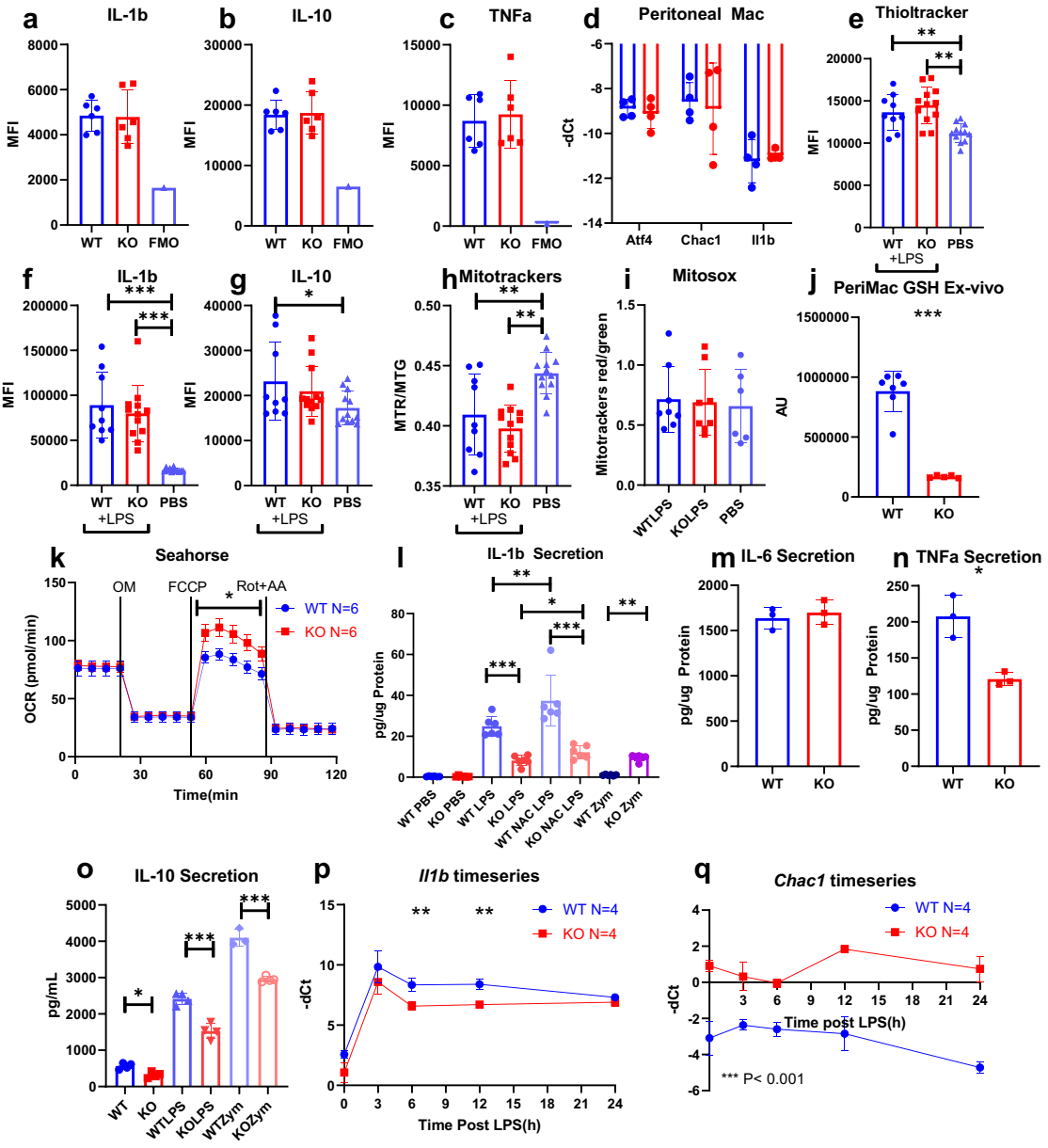


Figure 10 Peritoneal Macrophages (a-c) Intracellular cytokine staining (d) rtPCR analysis of sorted peritoneal macrophages, (e-i) Thioltracker, mitotracker, mitosox and intracellular cytokine staining in peritoneal macrophages from LPS-treated animals, (j) intracellular GSH of peritoneal lavage, (k) Seahorse of M1 polarized peritoneal lavage OM= Oligomycin, FCCP= Trifluoromethoxy carbonylcyanide phenylhydrazone, Rot= Rotenone, AA= Antimycin A, (l-o) Cytokine secretion, (p,q) LPS exposure expression timeline of Il1b and Chac1. Statistics: Student's t test; error bars represent SD; *p < 0.05, **p < 0.01, ***p < 0.001, for (k) T-test was performed for the average OCR per replicate per period between treatments, (p-q) multiple t-test with multiple testing correction was performed, (q) all timepoints had p < 0.001.

## 5.8 Peritoneal macrophages show no *in vivo* phenotype

To study the *in vivo* implications of sXc deficiency in macrophages, we isolated PMs from sXc KO mice and their controls. We found no differences in intracellular cytokine levels nor a difference in transcriptional levels of *Atf4, Chac1* and *Il1b* (fig 10a-d).
Animals were then treated with 2mg/kgbw LPS and peritoneal lavage was harvested 2

hours after injection. Thiol levels in macrophages from the peritoneal lavage were elevated after LPS treatment. Despite the increase in fluorescence upon activation, there was no observed difference between the groups (fig 10e). Intracellular cytokines were also assessed by intracellular cytokine staining. Although LPS induced an increase in intracellular IL-1b, there was no difference in intracellular cytokines between the groups (fig 10f,g). We then assessed mitochondrial membrane potential with mitotracker dyes and, although we did see a drop in membrane potential upon LPS treatment, we were not able to identify the two distinct populations we saw in BMDMs nor did we find a difference between genotypes (fig 10h). We also did not find a statistically significant difference in mitochondrial superoxide production (fig 10i). When peritoneal lavage GSH levels were measured immediately after isolation, we found a drastically lower GSH (fig 10j). Using Seahorse flux analysis, a standard mitochondrial stress-test was performed on peritoneal lavage stimulated for 24 hours with 100ng/mL LPS. We found increased oxygen consumption rates (OCRs) post FCCP treatment, indicating higher membrane potential. We then assessed cytokine secretion *in vitro* and found again lower cytokine production that could be partially improved by addition of N-acetyl-cysteine (fig 10l). Interestingly, zymosan, a TLR2 agonist that induces a respiratory burst in macrophages, increased IL-1b secretion only in KO macrophages. We also found lower TNFa and IL-10 secretion but no difference in IL-6 production (fig 10m-o). Finally we assessed *Il1b* and *Chac1* expression during 24 hours after LPS stimulation. We found lower levels of *Il1b* expression in KO peritoneal lavage at 6 and 12 hours post LPS stimulation and an elevation of Chac1 even before and throughout the LPS treatment indicating some level of cysteine shortage (fig 10p,g) that is not further increased by activation.

## 5.9 Dietary challenge exacerbates lack of insulin secretion and abolishes increased glucose uptake phenotype.

To investigate the implications of sXc deficiency upon a dietary challenge with high-fat diet (HFD), we fed the animals HFD for 4 weeks and assessed metabolic parameters by ipGTT (fig 11a,b,e,f). The previously observed increased glucose disposal in the ipGTT or eAT was no longer observed (fig 11g). The lower insulin secretion observed in KO mice seemed to be more pronounced in HFD fed animals with no difference in body weight (fig 11c). Additionally, this defect does not seem to be mediated by a lower beta cell mass (fig 11d). To investigate the abrogation of the increased glucose disposal in eAT, we isolated RNA from ATMs and performed rtPCR. To investigate a possible cysteine deficiency, we assessed *Chac1* expression but did not find a difference. Higher expression levels of *Il1b* (fig 11h,i) were found, suggesting a more pro-inflammatory phenotype in KO ATMs. We also isolated RNA from 3 different sorted islet fractions based on side scatter and CD45 positive antibody staining. We found elevated *Chac1* in both the beta cell enriched fraction as well as the immune cell fraction indicating cysteine shortage within the islets (fig 11j). We did not find an increase in *Il1b* (fig 11k).
To verify that this phenotype was a result of the dietary intervention, we phenotyped a small cohort of 12-week-old normal chow-fed animals and found no metabolic phenotype (fig 11l-p).

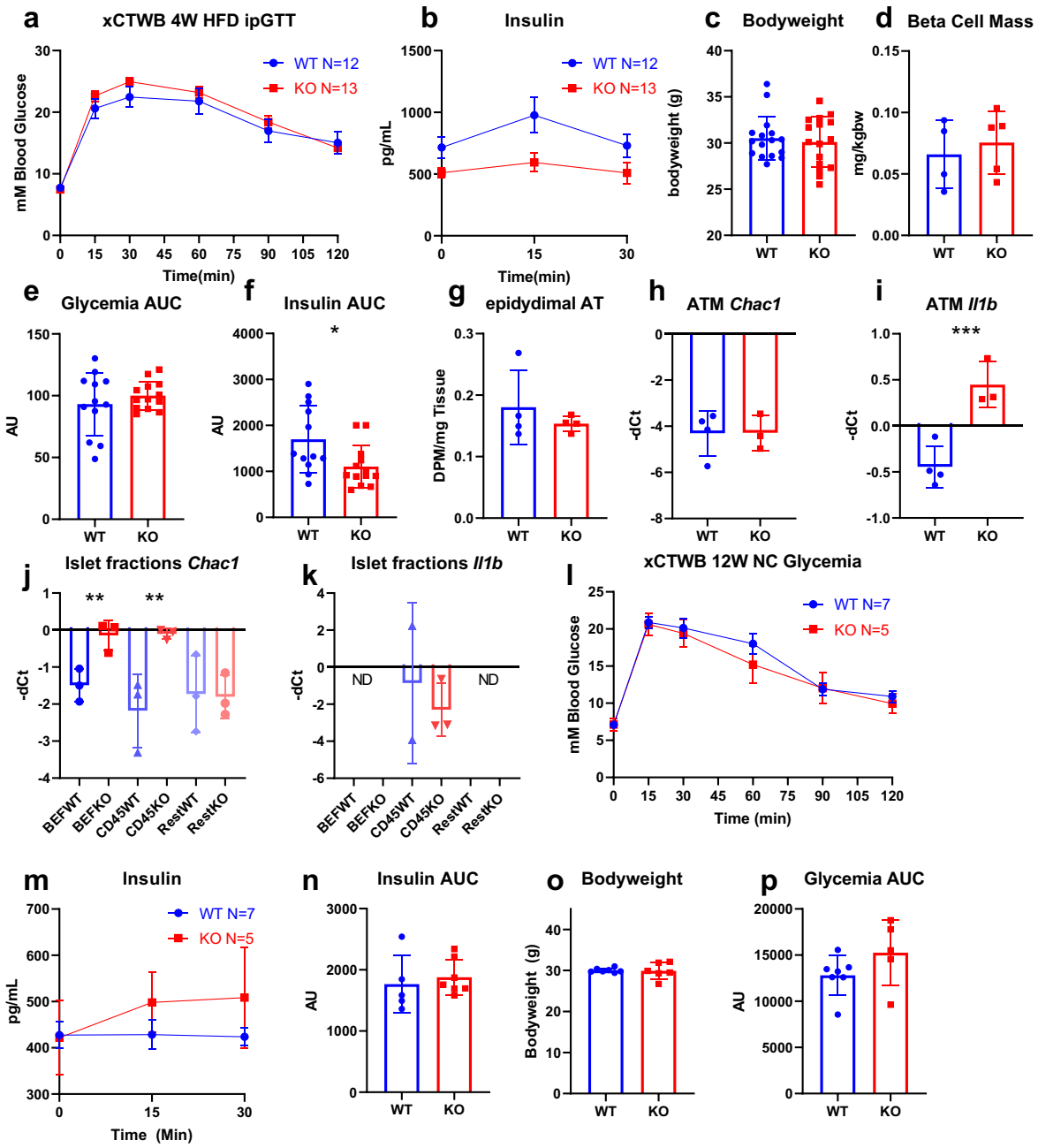


Figure 11 4 Week HFD fed whole body Slc7a11 knockouts (a) ipGTT glycemia, (b) Insulin, (c) Body weight, (d) beta cell mass (e) AUC of glycemia, (f) AUC of insulin, (g) 3H]2-deoxyglucose uptake in Epididymal Adipose Tissue, (h,i) rtPCR of sorted adipose tissue macrophages (j,k) rtPCR of FACS-sorted islet fractions (l) ipGTT glycemia, (m) Insulin, (n) AUC of insulin, (o) Body weight, (p) AUC of glycemia. Statistics: Student's t test; (a,b,l,m) error bars represent SEM, (c-k, n-p) error bars represent SD; *p < 0.05, **p < 0.01.

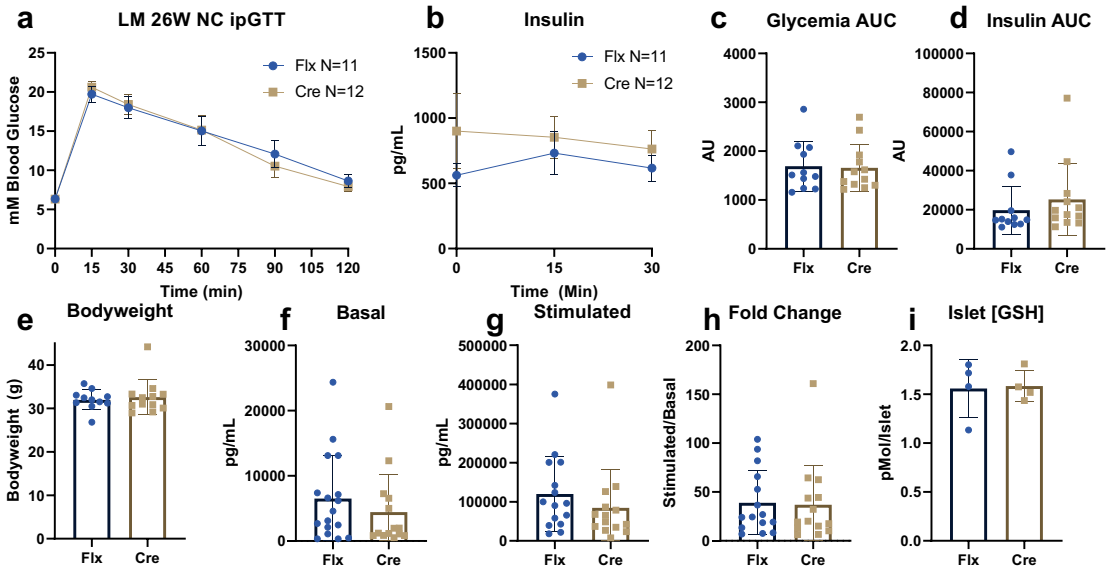


Figure 12 26-week-old LysM Cre Slc7a11 Flx (a) ipGTT glycemia, (b) Insulin, (c) AUC of glycemia, (d) AUC of insulin, (e) Bodyweight, (f-h) GSIS of isolated islets, (i) glutathione levels normalized per islet. (a,b,f-i) error bars represent SEM, (c-e) error bars represent SD.

## 5.10 Macrophage-specific sXc deletion does not phenocopy whole-body KO mice

To elucidate the macrophage-specific role of sXc, we crossed *Slc7a11* Flx mice with a myeloid specific LysM cre driverline to generate myeloid-specific sXc knockouts. The knockdown was verified by rtPCR of ATMs and sorted islet fractions. In the islets immune cells there is a knockdown of ~2 Cts corresponding to a ~75% knockdown, the expression levels of *Slc7a11* in the immune cell fraction is clearly higher compared to other islet fractions (fig 12g). The phenotype observed in the whole-body xCT KO line at 26 weeks of age was not present in the macrophage-specific mouse line (fig 12a-e).
To assess islet function *in vitro*, we isolated islets and performed a GSIS. We did not find significant differences in basal, stimulated or fold change in insulin secretion in these islets(fig 12f-h). Additionally, we measured glutathione, which was greatly reduced in whole-body KOs. In the myeloid specific knockout, we did not find a decrease in islet-wide GSH levels(fig 12i).

To observe the effects of a dietary challenge on myeloid sXc deficiency, mice were fed a HFD for 4 weeks after which an ipGTT was performed. Although it did not reach statistical significance, there seemed to be a trend towards lower insulin secretion in the knockouts (fig 13a,b,d,e). Beta cell mass was assessed and there was no significant difference observed and the body weight was also similar between genotypes (fig 13c,f). In ATMs there is also a decrease of about 2 Cts that is not observed in the non-macrophage fraction (fig 13h). We also determined *Chac1* and *Il1b* expression levels by rtPCR in sorted adipose tissue and PMs finding significantly higher expression of *Il1b* in PMs with a trend towards higher *Il1b* in ATMs (fig 13i,j).

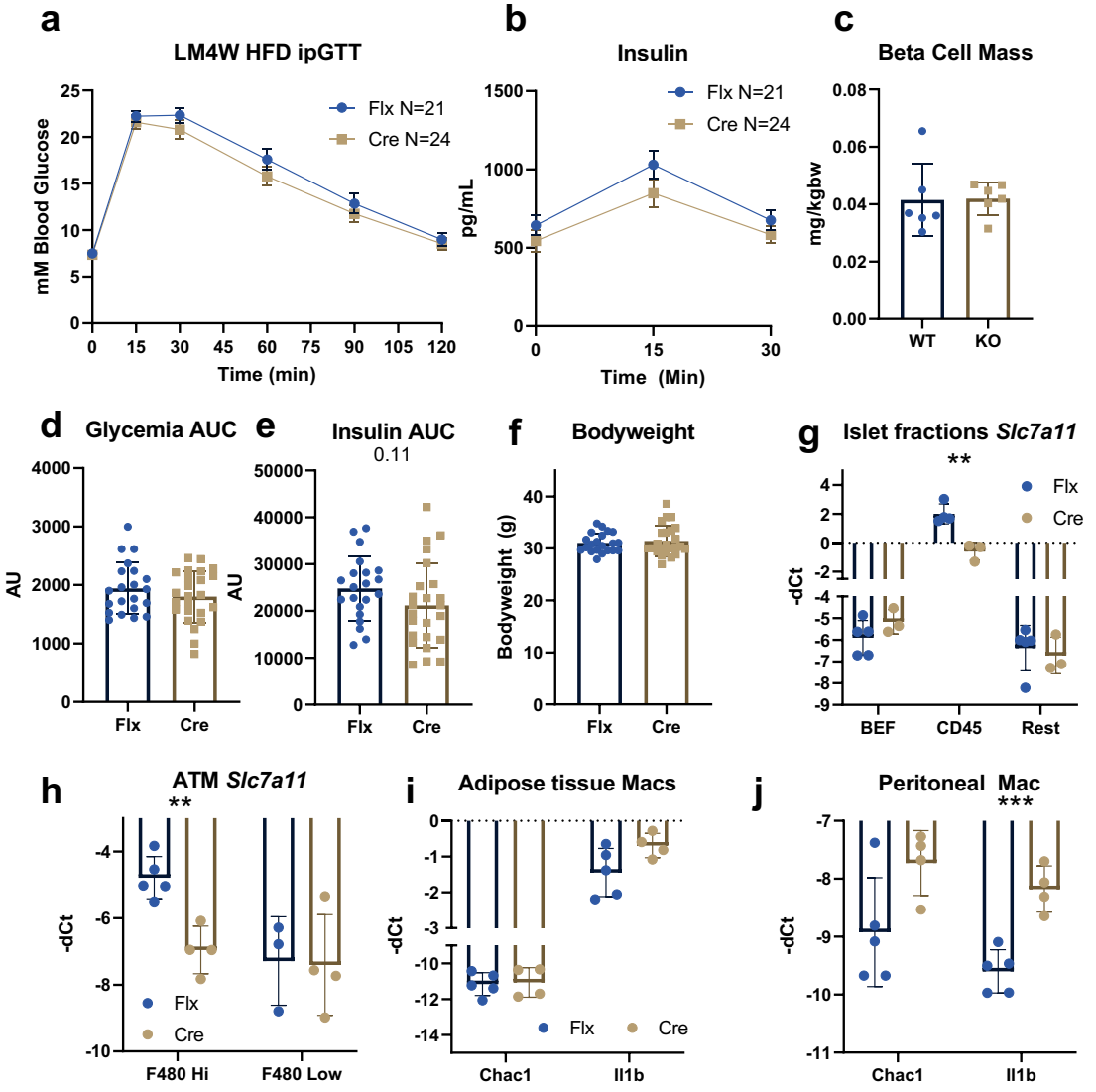


Figure 13 LysM Cre Slc7a11 Flx fed HFD for 4 weeks (a) ipGTT glycemia, (b) Insulin, (c) beta cell mass, (d) AUC of glycemia, (e) AUC of insulin, (f) Bodyweight, (g-j) rtPCR of sorted islet fractions, peritoneal and adipose tissue macrophages. Statistics: Student's t test; error bars represent SD; **p < 0.01, ***p < 0.001.

## 5.11 Long-term HFD does not precipitate a metabolic phenotype

To see if a longer dietary challenge would lead to decompensation, we assessed metabolic parameters again after 12 weeks of HFD feeding. We observed no differences in glucose disposal or insulin secretion between the experimental groups (fig 14a,b,d,e). We also observed no differences in body weight. Additionally, we performed an insulin tolerance test to see if there was a difference in insulin resistance but we did not observe an effect (fig 14f,g). We also screened peritoneal and ATMs with rtPCR for inflammatory cytokines and genes associated with cysteine shortage but found no significant increase after

correction for multiple testing (fig 14h,i).

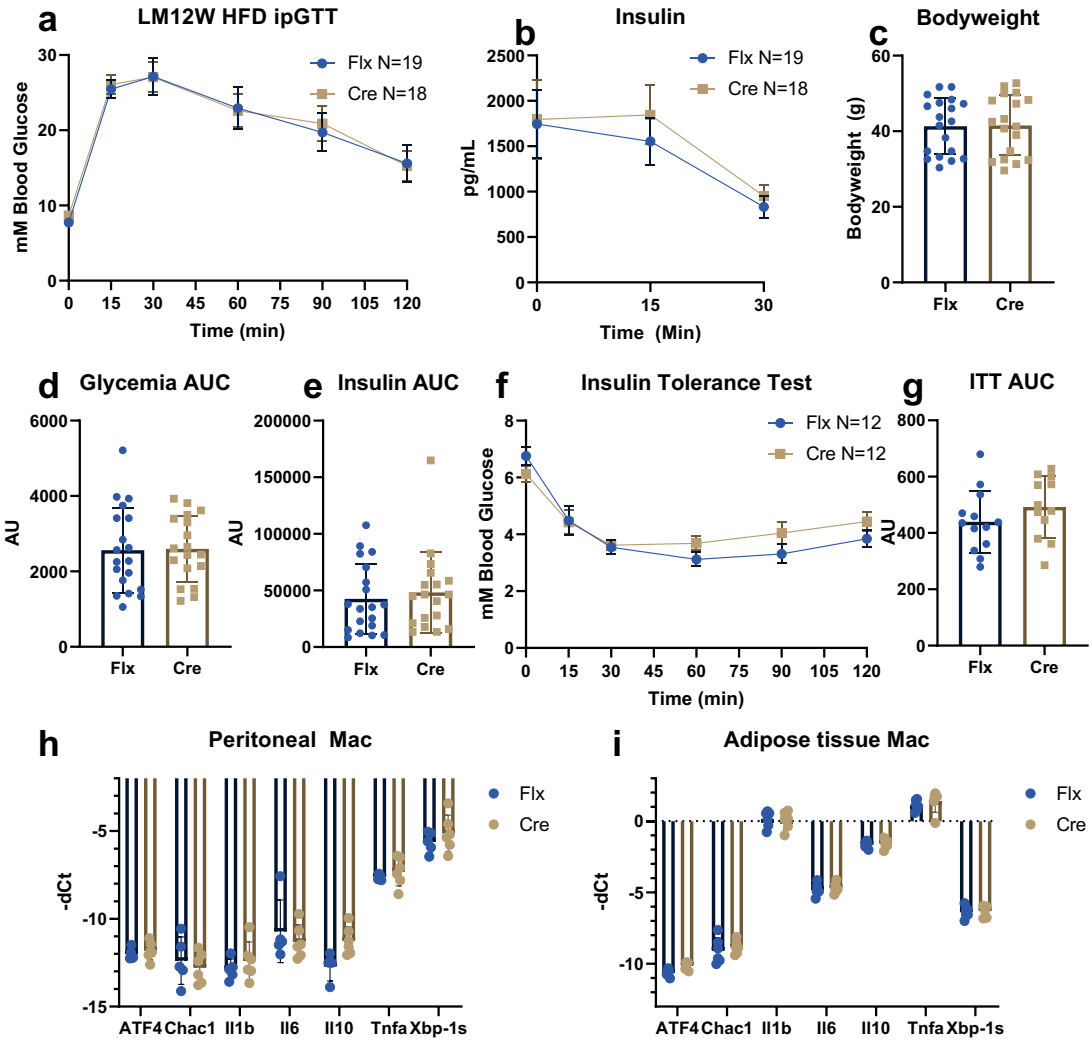


Figure 14 LysM Cre Slc7a11 Flx fed HFD for 12 weeks (a) ipGTT glycemia, (b) Insulin, (c) Bodyweight, (d) AUC of glycemia, (e) AUC of insulin, (f,g) insulin tolerance test, (h,i) rtPCR screening of sorted peritoneal and adipose tissue macrophages of mice fed HFD for 24 weeks. (a,b,f) error bars represent SEM, (c-e,g-i) error bars represent SD.

## 5.12 No sex-specific phenotype

In order to discover a potential sex-specific phenotype, we also assessed female macrophage-specific sXc knockout mice. The metabolic phenotype at 4 weeks of HFD was very similar to the male phenotype with a mild improvement in glucose disposal combined with a mild decrease in insulin secretion (fig 15a,b,e,f). There was no significant difference in body weight or beta cell mass (fig 15c,d). Similar to what we observed in male mice after 12 weeks of HFD, glycemia was identical between the groups. Additionally, there was a trend towards higher insulin secretion with similar body weights that did not reach statistical significance (fig 15g,h,j-l). An insulin-tolerance test (ITT) was performed to assess insulin resistance but no difference between the groups was observed (fig 15j,m). Finally, we assessed the beta cell mass of 8-week-old female mice before the dietary intervention and found it to be unchanged.

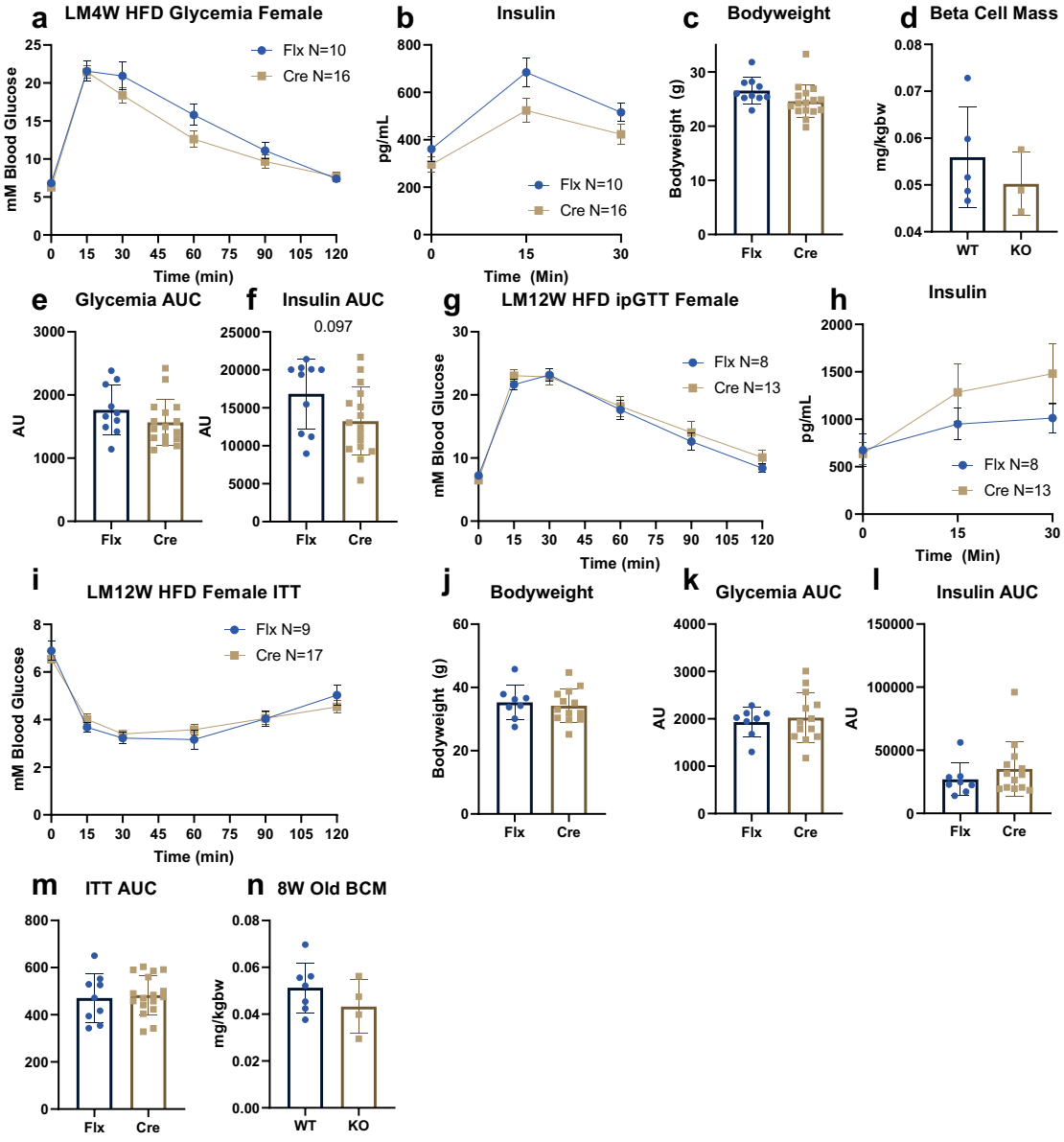


Figure 15 LysM Cre Slc7a11 Flx Females after 4 and 12 weeks of HFD & 8 weeks of age (a-f) ipGTT, bodyweight and beta cell mass of mice fed HFD for 4 weeks, (g,h,j,k,l) ipGTT and bodyweight of mice fed HFD for 12 weeks, (i,m) ITT of mice fed HFD for 12 weeks, (n) beta cell mass of 8 week old mice (before start HFD) . Statistics: Student's t test; (a,b,g-i) error bars represent SEM, (c-f,j-n) error bars represent SD.

# 6. Discussion

## 6.1 Whole body sXc knockout mice

In the present study we outlined the function of the cystine/glutamate transporter sXc *in vitro* as well as *in vivo* in the context of beta cell function and macrophage metabolism using sXc deficient mice.
At 12 weeks of age, sXc KO mice have metabolic parameters similar to WT controls. Later in life, at 26 weeks of age, sXc-deficient mice develop mild hypo-insulinemia. This suggests that the observed dysfunction is relatively mild and takes longer to decompensate. This late onset phenotype could implicate sXc as a contributor to aging, since ROS production and lower glutathione levels are associated with aging[106]. This could be further explored by screening beta cells for aging related genes and senescence associated secretory profile[107].
The observed lower insulin secretion is likely not only caused by lower beta cell mass, as only a small trend towards lower mass was measured. This suggests that there might also be a reduction in functional secretory capacity of the beta cells. The level of GSH within the islets was drastically decreased in sXc deficient islets. Since we found upregulation of *Chac1,* a glutathione degrading enzyme upregulated upon cystine starvation through Atf4, this could be a major factor driving down the islet glutathione levels.

When assessing insulin secretion by *ex-vivo* GSIS, we found drastically lower insulin output in *Slc7a11* KO islets, corroborating our *in vivo* findings, supporting an innate insulin secretory defect over a systemic adaptation. Addition of the glutathione pre-cursor γ-Glutamyl-Cysteine (GGC) was shown to abolish the difference in insulin secretion between WT and KO. It has to be noted however, that overall insulin output was significantly decreased in both groups by the treatment, possibly through ER stress by excessive reductive pressure[40] or GGC's anti-oxidative properties interfering with metabolic stimulation of insulin secretion[108].

Following this observation, one could argue for excessive redox stress due to GSH deficiency being a driver of beta cell dysfunction. We were not able to confirm this hypothesis using flow cytometry-based redox measurements in dispersed islets.
Ferroptosis has been reported in Islets treated with Erastin, and anti-ferroptotic agents improved the insulin output of transplanted islets *in vivo*[109], suggesting the beta cells might be sensitive to ferroptosis. Given the outcome of decompensated cysteine depletion induced redox stress being ferroptosis however[110], it is likely that these cells will quickly die and therefore be excluded from the analysis by live/dead staining.
Additionally, these dyes are not very sensitive, so it is possible SXc deficient beta cells are experiencing low-grade redox stress that can be compensated for and that is too subtle to measure with the currently employed methods.
These observations indicate that cells use glutathione not only for redox maintenance but also as a stockpile of cysteine, captured in a tripeptide which prevents export by other amino acid transporters. This stockpile can be tapped into by upregulation *Chac1* when the need arises. This is substantiated by the fact that sXc deficient cells do not massively decompensate into redox stress induced cell death, despite significantly lower GSH levels and *in vitro* culture. Further study could focus on other redox maintenance pathways such as the thioredoxin and glutaredoxin systems to explore the full extent of redox buffer depletion induced by sXc deficiency[111].

## 6.2 Cysteine shortage

Besides redox stress, shortage of cysteine could be another explanatory factor for the observed lower insulin secretion. Cysteine is a semi-essential amino acid, since it can only be synthesized through trans-sulphuration from the essential amino acid methionine[22]. This makes cysteine a limiting factor in many processes that has to be imported rather than generated. There are other amino acid transporters such as LAT1, ASCT2 and EAAT3[112] that can import cysteine derived from extracellular glutathione breakdown by γ-Glutamyl transferases (GGTs) and dipeptidases[113]. The import of its oxidized dimer cystine is restricted to sXc outside of the kidneys and intestinal tract. Moreover, the extracellular space has a high cystine/cysteine ratio, making it likely cystine uptake sXc significantly contributes to the intracellular cysteine pool.

Lack of sXc in beta cells leads to lower intracellular cystine, thereby cysteine levels. This leads to lower glutathione levels which could result in redox and ER stress that could interfere with insulin secretion. Less available cysteine also means reduced amounts of cysteinyl-tRNAs, which inherently could halt translation when that specific tRNA is needed. Moreover, GCN2 senses for tRNA availability and phosphorylates eIF2a when activated. This results in less transcription, which activates ATF4. ATF4 activates ATF3, which initiates the production of CHAC1. CHAC1 breaks down glutathione to provide cysteine for the cells, further depleting the glutathione pool. We did not find an upregulation of *Atf4* in sorted beta cells, which would be indicative of ER stress or tRNA shortage. We did find upregulation of *Chac1* in beta cells and islet immune cells, suggesting there is a compensatory response to the lack of sXc activity.

Lower cysteine levels could also decrease RAG1 and thereby mTORC1 activation, which results in lower production of insulin maturation factors such as CPE[114]. These pathways have been largely unexplored and could be further studied.

Another possibility that has not been explored is sXc functioning as a sort of "overflow valve". SXc activity involves the export of energetically valuable glutamate, combined with the import of cystine. Cystine requires immediate reduction upon import, consuming NADPH, increasing the energetic demand of sXc activity. This imposes a significant energetic debt on the cell. Reductive stress is a relatively new paradigm that could be especially relevant for beta cells, given their unrestricted glucose metabolism. The paradigm holds that excessive glucose flows lead to accumulation of reducing equivalents (NADH, NADPH) that result in the generation of reactive oxygen species and interference in mitochondrial metabolism[115]. System Xc activity could therefore move flow away from the mitochondria through glutamate export and consume reducing equivalents to alleviate reductive stress.

There is evidence that interactions between HATs and their shared heavy chain CD98 is a complex dynamic process of competing light chains for heavy chains during assembly. This process has also been described to involve regulators such as mTORC2[116] and CD44v[117]. Indeed, there has been a fascinating paper describing LAT1, a HAT that imports cyst**ei**ne, being downregulated in obesity[118]. This could be caused by an increasing oxidative islet micro-environment, perhaps combined with lower GSH production, leading to lower GSH degradation by GGTs[119] and therefore lower extracellular cysteine. Additionally, they described a role for CD44v in this process, that has been previously described by the authors themselves to stabilize sXc[117]. The authors indeed mention sXc in relation to LAT1 but show no experiments to substantiate their claim. This leads me to think they tried, but failed as there is no good commercial antibody out there for sXc[120]. It could be explored if *Slc7a11* deficiency leads to higher remaining LAT1 activity in beta cells during obesity.

Another feature we have observed at 26 weeks of age was a seemingly compensatory increase in glucose disposal. This leads to the paradoxical finding that, although the mice had lower levels of insulin, they more efficiently disposed of a glucose bolus administered during an ipGTT. This could be attributed to lower insulin levels throughout life, leading to increased tissue insulin sensitivity in KO animals. This hypothesis is supported *in vivo* by an increase in glucose uptake, using a radioactive glucose tracer. Whether this increase in uptake is mediated in an insulin dependent or independent way is not clear. To elucidate this, glucose uptake assays need to be performed without a glucose bolus as to not elicit an insulin response. We have generated supporting *in-vitro* evidence using isolated adipocytes, showing that knockout adipocytes are less responsive to insulin stimulated glucose uptake and have a trend toward higher basal glucose uptake, suggesting the effect might be insulin-independent.

## 6.3 Insulin resistance

The observed lower insulin secretion and increased glucose disposal, could also be explained by lower development of insulin resistance. This could be the result of lower cytokine production by tissue resident immune cells, that are known to induce insulin resistance by the production of cytokines[121]. This hypothesis is supported by our *in vitro* findings, showing impaired cytokine production in sXc deficient BMDMs. Cytokine production in macrophages, necessary for the development of insulin resistance, might also be impaired by sXc deficiency *in vivo* and thereby contribute to the observed phenotype.
In the adipose tissue of NC fed mice however, sorted ATMs did not show an upregulation of *Il1b* or *Chac1*, suggesting no activation or overt shortage of cysteine. PMs additionally did not show a difference in intracellular cytokine levels, with or without pre-stimulation with LPS *in vivo*.

When mice were given a dietary challenge in the form of 4 weeks HFD, the previously observed hypo-insulinemia of the KO mice compared to the WT mice was exacerbated. Despite the expansion induced by HFD, there was still no difference in beta cell mass, again supporting a functional defect not related to beta cell maintenance or expansion. Beta cells consistently had higher expression levels of *Chac1*, suggesting there was a certain degree of cysteine shortage, as well as in the immune cell fraction of the islets. One explanation for the disappearance of the increased glucose clearance in KO animals could be the more pro-inflammatory nature of ATMs in the KO animals. This pro-inflammatory nature could be induced by a combination of the aforementioned redox stress and cysteine shortage. This hypothesis is supported by the detection of higher expression levels of the pro-inflammatory cytokine *Il1b,* although we did not manage to find a significant increase in *Chac1* expression, which would indicate cysteine shortage.
ATMs have been described as a driver of adipose tissue insulin resistance[122]. HFD is well known to induce an inflammatory phenotype in macrophages and promote the recruitment of monocytes to the adipose tissue[123].
These findings make an *in vivo* macrophage functional defect preventing the formation of insulin resistance to explain the phenotype observed at 26 weeks of age appear less likely. Moreover, there are signs that sXc deficiency might even promote the development of insulin resistance during 4-week treatment with HFD, such as the trend towards higher glucose in the ipGTT, lack of difference in glucose uptake. and the increase in ATM *Il1b* expression.

## 6.4 System xC inhibitors

We also tested two sXc inhibitors in the context of insulin secretion namely: Erastin and Sulfasalazine (SSZ). Interestingly, the two inhibitors gave opposite results. Erastin significantly reduced insulin both after 24hour incubation as well as upon high glucose stimulation. This finding is corroborated by a publication investigating beta cell ferroptosis in the context of transplantation[109]. This could be explained by the many sXc independent activities of erastin[124]. For example, Erastin inhibits the voltage dependent anion channels on the mitochondria that are used to traffic TCA cycle substrates in and out of the mitochondria, inhibition leads to mitochondrial depolarization, which inhibits GSIS. Treatment of KO islets with Erastin resulted in lower GSH levels, this suggests that even the GSH lowering effect of Erastin might be occurring independently of sXc.
SSZ conversely had higher fold change in treated islets both in acute and incubation setting, albeit with lower basal insulin secretion. SXc inhibition by SSZ could induce insulin secretion by increasing intracellular ROS and glutamate, which both stimulate GSIS [102]. Supporting our findings is a case study of a patient with end stage renal disease that exhibited episodes of hypo-glycemia that were ablated upon SSZ treatment cessation[125].

## 6.5 Bone marrow derived Macrophages

To further study macrophage function, we investigated BMDMs and used a variety of *in vitro* techniques to assess various cellular processes that might be related to sXc. Macrophages generated from KO bone marrow showed several defects. KO macrophages had lower thiol levels, which is to be expected since cysteine is one of the main thiol carrying compounds within the cell, either as free cysteine, GSH or incorporated in proteins. Cytokine production was also significantly diminished for IL-1b and IL-10. This could be caused by a combination of redox stress and cysteine shortage. We indeed find increased *Chac1* expression in PMs *in vitro,* but we did not find increased ROS in KO macrophages (data not shown). It could be investigated whether this lack of cytokine production is because of reduced mTORC1 activation, which is vital for cytokine production and can be inhibited by cysteine shortage[126]. Intracellular cytokine staining paradoxically showed higher intracellular levels of IL-1b and IL-10 in BMDMs. IL-1b is present in the cell as pro-IL-1b until it is cleaved by caspase 1 located on an activated NLRP3 inflammasome. After cleavage, IL-1b can either be released through microvesicles and exosomes or membrane pores such as gasdermin-D, depending on the strength of the inflammatory stimulus[127]. Since cleavage is required for secretion, sXc deficient macrophages might have reduced caspase-1 activity leading to accumulation of pro-IL-1b. The antibody used cross-reacts with pro and mature IL-1b, which means we will not be able to assess this using our flow cytometry-based approach. Macrophages build up intracellular pro-IL-1b levels after a primary stimulus such as LPS. After this initial accumulation a second hit such as ATP is required to trigger IL-1b maturation and release from the macrophage. Interestingly, a 1-hour 2mM ATP treatment did not decrease cytokine fluorescence in BMDMs, suggesting that the total release of cytokine during the 1-hour time-period is not enough to result in a significant decrease of the intracellular cytokine pools detectable by intracellular cytokine staining.
IL-10 is a soluble cytokine that gets secreted in the conventional pathway, being trafficked from the trans-Golgi-system in secretory vesicles. There is therefore not a specialized mechanism for the activation or secretion. The current literature states that the secretion of IL-10 is more of a stochastic process regulated by cytokine production without any

additional specialized regulatory mechanisms such as inflammasome activation[128]. Despite this, IL-10 shows the same pattern of cytokine accumulation as IL-1b.
Another explanation for both the accumulation of IL-1b and IL-10 therefore could be a defect in the trafficking and production of the cytokines, leading to congestion in the ER or Golgi. This would appear as higher cytokine intracellular cytokines combined with lower secretory output, as we observe in the KO BMDMs.
Since mitochondria play a pivotal role in cell metabolism, we assessed their function in resting and activated macrophages. The mitochondria of KO macrophages showed lower flexibility in terms of regulating membrane potential resulting in low MP populations. KO macrophages had higher MP and in high MP populations, KO macrophages trended towards lower MP. This suggests lower mitochondrial flexibility in response to LPS, which is also seen by mitochondrial superoxide production. The macrophages have an overall higher superoxide production, likely due to the impaired redox buffering capacity. WT BMDMs show flexibility in superoxide levels, dropping in response to LPS treatment and drastically increasing upon Zymosan treatment. These changes are less pronounced in KO BMDMs.
SXc could have a fundamental role in mitochondrial changes occurring upon macrophage activation. This hypothesis would fit the rapid upregulation upon LPS stimulus and its transporter activity. Intracellular cysteine is known to activate pyruvate dehydrogenase kinase 2[129], which reduces flux into the TCA cycle. Additionally, glutamate export could indirectly drain the TCA cycle by anaplerosis of 2-oxoglutarate, which would also result in lowered membrane potential. The inducible nature of the transporter makes it a likely upstream effector of metabolic changes in macrophages upon LPS stimulus.

## 6.6 Peritoneal Macrophages

To confirm our *in vitro* findings with BMDMs, we decided to investigate at macrophages *in vivo.* To minimize confounding effects and the isolation time, we decided to use PMs as a model because they can be easily isolated, without digestion, by peritoneal lavage. When we measured the glutathione levels of peritoneal lavage it was drastically reduced; interestingly we did not observe increased *Chac1* expression, which would be an indicator of cysteine starvation. Likewise, we did not find a difference in intracellular cytokines, thiol levels or superoxide either, with or without LPS stimulus. We also did not find the separation into high MP and low MP population observed in BMDMs, and overall membrane potential was not changed.
After 24 hour *in vitro* LPS treatment, we did observe higher reserve capacity as evidenced by OCR when treated with FCCP in the seahorse assay in KO PMs. This matches the higher MP observed in BMDMs.
The only differences we found were after 24hour *in vitro* incubation, mirroring many of the phenotypes we have found in BMDMs, indicating that these effects might be a result of the differences between *in vivo* and *in vitro* conditions.
It is well known that cell culture conditions are more oxidative that the *in vivo* milieu[111]. The import of cysteine's oxidized dimer cystine makes sXc especially important in the context of an oxidizing extracellular environment, where more of the cysteine pool will be oxidized to cystine. Additionally, there are NRF2 binding motifs upstream of *Slc7a11* which regulates its expression upon disturbances in redox homeostasis.

Despite our *in vitro* evidence of lower cytokine levels, we did not find a difference in serum IL-1b levels 6 hours post injection. Neither did we find a difference in whole blood glutathione levels in response to a LPS stimulus, despite reports of lower serum GSH in these animals[105]. Although LPS pre-injection abrogated the difference between WT and KO in the ipGTT, it had such a profound effect on metabolic parameters that the results are of limited interpretive value. Lack of *in vivo* translatability of a sXc phenotype has been reported before in a paper describing that sXc is required for *in vitro* expansion of T-cells, while finding no evidence of decreased T-cell proliferation *in vivo*[130].

LPS treatment could be sub-optimal for eliciting a phenotype in these animals. Zymosan has been described to induce a respiratory burst in macrophages and induces an increase in mitochondrial superoxide production, which could make intracellular GSH levels more important[132]. Additionally, zymosan induced IL-1b production only in KO PMs.

## 6.7 Myeloid specific system Xc- knockout mice

The high *Slc7a11* expression levels of islet immune cells compared to other islet fractions, prompted us to generate myeloid specific *Slc7a11* knockouts to study the myeloid-specific role of *Slc7a11* in the observed reduction in insulin secretion. At 26 weeks of age, we did not observe the previously observed phenotype in whole body knockouts. This might suggest the insulin secretory phenotype is mediated mostly by sXc deficiency in other islet cells, most likely beta cells, and that the increased glucose disposal might be secondary to the lower insulin secretion. Additionally, islets isolated from these animals did not have lower GSH levels, nor did they have decreased GSIS.
When given 4 weeks HFD, insulin secretion trended to be lower in the KO animals but it failed to reach statistical significance. The same effect was also observed in female mice, supporting the existence of a very mild insulin secretory defect in these animals, given the equal levels of beta cell mass.
When myeloid-specific Slc7a11 KO mice were kept on HFD for 12weeks, the previously observed mild phenotype was no longer observable. This fits a common pattern in mouse metabolic phenotypes that are either severe enough to completely decompensate over time or mild enough for the metabolic system to adapt and compensate to the disturbance induced by a certain gene defect/intervention.

The data from the myeloid-specific knockouts suggests that hypo-insulinemia is not due to myeloid cell-derived signals acting on beta cells. One hypothesis we formulated was that macrophages might be contributing to the whole islet GSH pool. However, sXc KO and wild-type controls showed similar levels of GSH in the islets disproving this hypothesis.
We have shown that KO BMDMs indeed secrete less GSH into their culture medium and the overall reductive potential of the medium is lower in medium cultured with KO macrophages.
Moreover, we performed medium transfer GSIS with medium conditioned by WT and KO BMDMs but did not find a difference, suggesting there is limited sXc facilitated cross-talk between beta cells and macrophages.
We did not find a difference in beta cell mass either, which excludes a role of myeloid cell sXc in islet expansion. This is of importance because excessive glutamate as observed in beta-cell lines exposed to high glucose enhances apoptosis[103], the effect being mediated by NMDA receptor signalling. NMDA receptor inhibition has also been shown to increase the depolarization plateaus observed during insulin secretion, leading to higher insulin output and better glucose disposal[131]. Furthermore, sXc in macrophages has been implicated as

the main culprit in glutamate induced neurotoxicity[32]. These data therefore suggest that macrophage sXc does not contribute to glutamate induced excitoxicity of beta cells.

## 6.8 Conclusion

This thesis outlines the role of sXc in macrophages and islet function. We have shown that sXc is vital for maintaining normal GSH levels in the cell, in macrophages and islets. Despite drastically lowered GSH levels, cells remain viable and even have similar staining levels with thiol specific dyes, suggesting even overall thiol levels in the cell are relatively unaffected. Despite the drastic reduction in GSH, the mice seem completely healthy and no decompensating phenotype emerges. We have however shown that whole body sXc deficiency leads to insulin secretory defects *in vivo* as well as *in vitro*. This suggests that beta cells might be especially sensitive to sXc deficiency, either through high sensitivity to redox stress or cysteine demand.

Because of the relatively high expression levels *Slc7a11* in islet immune cells, we speculated it might be islet macrophages that were responsible for the observed phenotype. Myeloid specific *Slc7a11* KOs unfortunately produced an even more subtle, arguably non-existent, phenotype, which did not translate *in vitro*. These findings suggest that the observed insulin secretory phenotype is not mediated by myeloid cells and might be a beta cell intrinsic phenomenon, despite low relative expression of *Slc7a11*. Based on these data, we can also exclude islet macrophage sXc as contributing to islet dysfunction as a result of glutamate induced excitotoxicity, in the contexts we investigated.

Bone marrow derived macrophages from KO animals showed clear metabolic and functional defect, likely caused by cysteine shortage. For further investigation, the metabolome of BMDMs could be explored to investigate the impact on the overall metabolism of not having the import of cystine and export of glutamate by sXc, with and without activation by LPS. Additionally, cytokine production and secretion pathways could be investigated, to explain the paradoxical finding of increased intracellular cytokines. The findings made *in vitro* using BMDMs could not be translated *in vivo* however, suggesting that *in vitro* culture conditions might be a causal factor in the observed BMDM and PM phenotype.

Overall this project shows the importance of cellular redox maintenance, since many overlapping mechanisms have evolved leading to a robust system that is only minorly disturbed by an arguably quite important and unique transporter. This results in a relatively mild phenotype requiring large sample sizes to reach statistical significance during most metabolic experiments. This makes additional experiments to understand the underlying mechanisms more difficult. Especially when the causation is multifactorial, with many different factors contributing in a minor fashion that doesn't result in big effect sizes by themselves. *In vitro*, the phenotype was much more robust but hard to reproduce *in vivo*, making the degree to which findings *in vitro* are translatable uncertain.

# 7. Materials and methods

## 7.1 Mouse Models

All animal experiments were conducted according to the Swiss Veterinary Law and Institutional Guidelines and were approved by the Swiss Authorities. All animals were housed in a temperature-controlled room with a 12 h light–12 h dark cycle and had free access to food and water. Given the propensity of males to develop metabolic dysfunction, for most experiments males were used.
C57Bl6NCrl mice were used as wild-types and generated from our own in-house colonies. Constitutive *Slc7a11* knockout mice were first generated by Sato et al. on a C57Bl6J background and were maintained in our in-house colony. A GFP cassette inserted into exon 1 of the *Slc7a11* is used to generate whole-body knockouts. Animals were propagated using het-to-het breeding in order to ensure littermates represented in both experimental groups.

C57Bl/6N Slc7a11<tm1(EUCOMM)Wtsi/IcsOrl> were acquired from INFRAFRONTIER GmbH. To generate
Conditional myeloid specific *Slc7a11* knockout mice were generated by crossing our B6.129P2-Lyz2<tm1(cre)Ifo>, acquired from Jackson and backcrossed to C57Bl6N background, with  The resulting mouse line did not exhibit any observable developmental defects. Knockdown efficiency was assessed by rtPCR.

## 7.2 Endotoxemia

To induce endotoxemia, mice were injected with PBS containing 2mg/kg body weight phenol-extracted LPS (*Escherichia coli* O26:B6, Sigma-Aldrich). Mice were monitored regularly during the 2-8 hours before sacrifice or metabolic experiment.

## 7.3 Metabolic phenotyping

For the intraperitoneal glucose tolerance test, mice were fasted for 6 hours (from 8AM until 2PM) and then injected with 2g/kg body weight glucose with a 40% glucose solution. Blood glucose was monitored at the 0, 15, 30, 60, 90 and 120 minute timepoint post injection using a Freestyle Lite Glucometer form Abbott. Additionally at the 0, 15 and 30 minute timepoint, 25 uL of blood was collected in tubes containing 2.5 uL of 50mM EDTA solution to obtain plasma for insulin measurements.
Insulin resistance was assessed by insulin tolerance tests where mice were injected with 1 (1.5 for high fat diet fed mice) U/kg body weight Actrapid from NovoNordisk, glucose is measured at the 0, 15, 30, 60, 90 and 120 minute timepoint post injection using a Freestyle Lite Glucometer from Abbott.

## 7.4 [3H]2-deoxyglucose uptake and detection

To assess glucose uptake by tissues, mice were fasted for 6 hours and injected with 2g/kgbw 40% glucose solution spiked with 350 uCi/kgbw [3H]2-deoxyglucose acquired from Perkin Elmers. Tissues were harvested and 200 mg of the respective tissue was taken and homogenized in 500 uL ultra-pure water with a stainless-steel bead in a TissueLyser II from Qiagen. The homogenate was then heated in a heating block at 95 C and subsequently spun down at max speed for 5 minutes. Supernatant was collected and phosphorylated 2-[3H] deoxyglucose was separated by Poly-Prep columns (#731-6212, BioRad). The final eluate was mixed with Ultima Gold Scintillation fluid at a 1:7 Ratio in scintillation tubes and was analysed with a beta counter.

## 7.5 Adipose tissue isolation

Epidydimal white adipose tissue was isolated and minced with scissors. The adipose tissue was then incubated with collagenase for 45 minutes at 37 C in a shaker. Stromal vascular fraction was obtained through centrifugation and, after incubation with red blood cell lysis buffer, subsequently sorted by FACS, gating for Lin- CD11b+ and F480+ cells.
If adipocytes were isolated, the digested adipose tissue was spun at 30 g, the infranatant was removed, the floating fraction was washed and filtered through a 200 um pore size mesh. Adipocytes were then distributed for experiments based on volume.

## 7.6 Ex-vivo adipocyte 2-DG uptake

To assess glucose uptake in isolated adipocytes, Promega glucose-uptake glo assay based on 2-DG was used. In short, isolated adipocytes were distributed upon volume in glass tubes in a 37 C shaker in Krebs ringer buffer containing 11mM Glucose and 1mM 2-DG. After shaking incubation for 1 hour, cells were processed according to manufacturer's protocol.

## 7.7 Peritoneal macrophage isolation

For the isolation of peritoneal macrophages, peritoneal lavage was obtained by flushing the peritoneal cavity with PBS containing 0.5% BSA and 5mM EDTA. The lavage was then collected through a glass funnel in a tube topped with a 70 uM strainer. Cells were then centrifuged and taken for further processing.

## 7.8 Islet isolation

Islets were isolated by collagenase digestion through infusion of collagenase mix through biliopancreatic duct. Islets were harvested by handpicking under a microscope and cultured in a cell culture incubator (37C and 5% C02) in DMEM (GIBCO) containing 11.1 mM glucose, 1mM Pyruvate, Non-Essential Amino Acids (GIBCO), 100 units/ml penicillin, 100 µg/ml streptomycin, 2 mM Glutamine, 50 µg/ml gentamycin, 10 µg/ml Fungison and 10% FCS.

## 7.9 Glucose stimulated insulin secretion

GSIS was adapted from an earlier publication (citation). In short, islets were incubated in 96 well plates with 1 islet per well that were size-matched between groups for 2-3 days in a cell culture incubator in DMEM (GIBCO) containing 11.1 mM glucose, 1mM Pyruvate, GIBCO Non-Essential Amino Acids, 100 units/ml penicillin, 100 µg/ml streptomycin, 2 mM Glutamine, 50 µg/ml gentamycin, 10 µg/ml Fungison and 10% FCS.
Following the incubation, islets were washed and then pre-incubated for 90 min in preequilibrated Krebs-Ringer bicarbonate buffer (KRB; 115mMNaCl, 4.7mMKCl, 2.6mMCaCl2 2H2O, 1.2mMKH2PO4, 1.2mMMgSO4 7H2O, 10 mM HEPES, 0.5% bovine serum albumin, pH 7.4) containing 2.8 mM glucose. The medium was then changed again and incubated for 1 hour to obtain the samples for basal secretion, subsequently the medium is exchanged for 16.7mM high glucose KRB which will yield the stimulated sample. After the experiment, wells were checked by eye and wells not containing an islet were excluded. Five wells were pooled and insulin was quantified with the mesoscale mouse/rat insulin assay (Meso Scale Diagnostics LLC). Stimulation index was calculated as the division of stimulated by basal secretion.
For medium transfer experiments, medium was conditioned for 2 days in a petri dish seeded at 10^6 cells/mL sometimes pre-conditioned with 100 ng/mL LPS for 1 day. The medium was then collected, spun down and then incubated with the islets for 24 hours.

## 7.10 RNA Isolation and rtPCR

RNA was isolated by the Nucleo Spin RNA II Kit (Machery Nagel, Düren, Germany). cDNA was prepared with the GoScript Reverse Transcription Mix containing random primers

(Promega AG) according to the manufacturer's instructions. For quantitative rtPCR of *Chac1*, *Il1b* and *Slc7a11* SYBRgreen-based chemistry with GoTaq Polymerase (Promega AG) and the ABI 7500 fast system (Applied Biosystems) was employed. Hprt was used as a housekeeping gene and expression levels were calculated as –(GOI-HKG) as to not assume an amplification efficiency of 2 and to display the data in the most unadulterated manner. Primer sequences were all derived the first ranked pairs in the Harvard Primer Bank https://pga.mgh.harvard.edu/primerbank/.

## 7.11 Bone marrow derived macrophages

To prepare bone marrow derived macrophages, both hindlegs of 16-26-week-old mice were harvested and stripped to the bone. Then both the tibia and femur are cut on both ends and flushed with DMEM (GIBCO) containing 11.1 mM glucose, 1mM Pyruvate, GIBCO Non-Essential Amino Acids, 100 units/ml penicillin, 100 µg/ml streptomycin, 2 mM Glutamine, 50 µg/ml gentamycin, 10 µg/ml Fungison, 50 uM beta-mercapto-ethanol, 50 ng/ml M-CSF (Biolegend) and 10% FCS (BMDM medium). The cells were then cultured in BMDM medium in 9cm bacterial culture dishes (Sarstedt) at a density of 10^7 cells per dish. Medium changes were performed at 3 and 6 days after the start of the culture. At day 8 the cells are harvested by incubation at 4 C for 10 minutes in PBS + 0.5% BSA + 5mM EDTA, washed with fresh medium and subsequently polarized with LPS SM (100ng/mL)(InvitroGen), IL-4 (20ng/mL)(Biolegend) or oxPAPC(50ug/mL)(Polaris) in BMDM medium for 6-24 hours.

## 7.12 Flow cytometry

Flow cytometry experiments were performed on a CytoFLEX V2-B4-R2 Flow Cytometer (8 Detectors, 3 Lasers) (Beckman). In short, cells were harvested as previously described and subsequently stained with the appropriate antibodies and dyes. For flow cytometry experiments, F4/80 APC-Cy7 and CD11b PE-Cy7 (Biolegend) positive cells were considered macrophages.

To determine membrane potential of the mitochondria, Mitotracker Red FM and Mitotracker Green FM (ThermoFisher) staining was performed in 100 nM concentration for both dyes according to manufacturer's protocol, cells were stained in DMEM with BSA instead of FCS. The cells were not washed after staining and immediately acquired after incubation in the staining buffer. The average membrane potential per mitochondrion was calculated as mitotracker red/mitotracker green.

To quantify mitochondrial super-oxide production, MitoSox Red and Mitotracker Green FM (ThermoFisher) staining was performed in 100 nM concentration for both dyes according to manufacturer's protocol, cells were stained in DMEM with BSA instead of FCS. The cells were not washed after staining and immediately acquired after incubation in the staining buffer. The average membrane potential per mitochondrion was calculated as mitosox red/mitotracker green.

For measuring intracellular thiol levels, Thioltracker dye (ThermoFisher) was used according to manufacturer's directions. Cells were washed and subsequently analysed.

## 7.13 FACS sorting of macrophages and dispersed islets fractions

After isolation, islets were washed in PBS and resuspended in a 0.5% trypsin + EDTA solution (GIBCO) at a final concentration of 0.01%. For dispersion of islets into single cells, samples were incubated at 37°C for 90 s, with mechanic up and down pipetting every 30 s. Trypsin activity was stopped by filling the tube with ice-cold FACS buffer (PBS +0.5% BSA + 5mM EDTA). Then cells were washed, resuspend in 100 µL FACS buffer and processed for staining and FACS sorting. To avoid unspecific binding, cells were incubated at 4°C for

15 min with anti-CD16/CD32 (Biolegend), then with anti-mouse CD45 APC antibody (eBioscience) for 30 min in the dark on ice. After staining, cells were sorted on the FACSMelody (BD). Beta cells mice were sorted based on size and granularity as described before[133] and islet immune cells were sorted as the CD45+ fraction.
Macrophages from different tissues were identified as F4/80 PE-Cy7 and CD11b PerCP-Cy7 (Biolegend) positive cells after being gated for Lineage negative(CD19, Ly-6G, CD3, NK1.1, BV510 Biolegend) singlet and DAPI negative live cells. The cells were sorted on the FACSMelody (BD).

## 7.14 *In vitro* IL-1b/IL-10 secretion assay

250'000 cells/well were cultured overnight in 250 ul of medium in a 96 well plate?. Cells were washed with warm PBS and treated for 23 h with or without LPS at a concentration of 100 ng/mL (InvivoGen, tlrl-smlps, LPS from S. minnesota R595). To further stimulated secretion, ATP (InvivoGen) was added at a concentration of 2 mM for 60 min prior to collection of culture supernatants. IL-1beta concentrations in cell culture supernatants were measured using MSD mouse IL-1beta assay kit (K152QPD; Meso Scale Discovery) and normalised to protein content as measured by BCA assay (ThermoFisher). IL-10 was assessed using a standard IL-10 ELISA according to manufacturer's protocol (Biolegend).

## 7.15 ATP, Glutathione and redox potential measurement

ATP Measurements were performed using Promega CelltiterGlo3D. For glutathione measurements in islets, an adapted version of the GSH-glo assay (Promega) was performed where the standard lysis buffer was replaced with passive lysis buffer (Promega) in order to prevent inadequate permeabilization. Ten islets were size matched and moved into a well containing 100 uL reaction mix.
For glutathione measurements in BMDMs, 100 000 cells were plated in a well of a translucent bottom 96 well plate. The assay was performed according to protocol. For glutathione measurements of medium, 50 uL cultured medium was combined with 2X reaction mix and analysed according to protocol. Medium redox potential was measured from the same samples using antioxidant assay kit (MAK334, Sigma-Aldrich).

## 7.16 Microscopy and beta cell mass quantification

The weight of the pancreas was determined at sacrifice. To measure the beta cell mass and mean islet area, pancreata were fixed in 4% buffered formalin at 4 C overnight and embedded in paraffin. Organs were cut with an electronic rotary Microtome, Microm HM 340E. As soon as a representative area of the organ was reached, five 5-um-thick sections were collected. Thereafter, 100 mm were trimmed and then again five 5-um-thick sections were collected. This was repeated so that in the end three to four representative sections from different depths of the pancreas could be further deparaffinised and re-hydrated. For insulin staining, the slides were incubated with a guinea pig anti-insulin antibody (Dako, A0564) for 2h at room temperature, followed by an overnight staining at 4_C with a rat anti-CD45 antibody (BD Pharmingen, 550539) to detect lymph nodes. The next day, the slides were incubated consecutively with Alexa Fluor 647-conjugated goat anti–guinea pig IgG (Invitrogen, A21450) and Alexa Fluor 555-conjugated goat anti-rat IgG (Invitrogen, A21434), each for 2h. Cell nuclei were stained with DAPI and sections were mounted with mounting medium (Dako, S3023). For image acquisition a Prior PL-200 slide loading robot and an automated Nikon EclipseNi microscope with a Hamamatsu flash 4.0 camera and a 4x Nikon Objective NA 0.2 was used.

Pancreas and beta cell area were determined using a convolutional neural network approach using the U-net architecture from https://github.com/jvanvugt/pytorch-unet. The outputs were hand curated and analysed using ImageJ software. Normalized beta cell weight was calculated as ratio (beta cell area/pancreas area)*(pancreas weight/bodyweight).

## 7.17 Data analysis

Results were analyzed with Prism 9.1.0 (GraphPad, USA) or Python and Jupyter notebook (Jupyter Labs), $p < 0.05$ was considered to be significant. Results were expressed as mean ± SEM or SD. Data were analyzed with unpaired Student's t test or Sidak's multiple comparison test. Statistical details of experiments can be found in the figure legends and in the figures.

# 8. Acknowledgements

I would like to thank Marc Donath for giving me the opportunity of pursuing a PhD in his lab. I am extremely grateful for allowing me the independence and room to make and learn from my own mistakes. I also highly appreciate your genuine concern, optimism, support and guidance throughout my PhD.

I would also like to thank Christoph Hess for agreeing to be on my PhD committee and giving me advice on exploring macrophage immunometabolism. Additionally I would like to thank Philippe Dehio and Jasmin Graehlert from the Hess lab for sharing reagents and showing me some techniques.

Thanks to Daniel Konrad for being my external supervisor and providing valuable feedback during the committee meetings.

Many thanks to Marianne Böni-Schnetzler for being an example of scientific rigor and an endless source of knowledge. I am also eternally grateful that you alerted me to the need of flipase recombination in my the floxed mouse line and subsequently procured those mice for me. You prevented a disaster that could have cost me many months of time.

I am thankful for Adriano Fontana for suggesting the initial idea for the project, providing feedback on the manuscript and attending all of my group meetings and discussions regarding the project. I also appreciated our shared interest in Dostoyevsky. Your suggestions and discussions have been fundamental to my understanding.

I consider myself extremely lucky to have spent my PhD in a lab with such a good atmosphere and great people both professionally and socially. I consider you all my friends.
Daniel has given me a lot of useful feedback over the years both scientifically and about how to approach my PhD. I would also like to thank him for the feedback on the manuscript.
Many thanks to Josua who has been a great friend over the years and managed to single-handedly keep my social life from disappearing completely during the course of my PhD. He has also been an excellent guide to the party scene in Basel.
Thanks to Sophia for bringing the competitive spirit and the thought-provoking discussions.
Thanks to Leila for helping me with many of the larger experiments and spending many hours in the experimental room helping me with GTTs and sharing stories about your cats.
My thanks go out to Stephie getting me acquainted with the lab when I first arrived.
I would also like to thank Hélène for the help with experiments and discussions of French cuisine.
Thanks to Joyce for being an exemplary scientist, it has been an inspiration seeing you progress in your project.
My admiration goes out to Laura who has garnered the courage to tackle the project I could not. I am convinced you will persevere! Thank you for being a constant source of enthusiasm in the lab.
Thank you Kelly sharing memes and all the discussion about the different mechanisms of insulin secretion.

I will be eternally grateful for all the emotional and dietary support provided by Jeanne, in addition to giving me the no-nonsense perspective of a world-class doctor.

Thanks to Mo for the friendship and keeping me connected to my Dutch roots while in Switzerland. I really enjoyed doing the blockchain challenge together and the many nights hanging out and discussing philosophy.

Thanks to Maarten, Boudewijn, Benjamin and all the other men from the house. I would also like to thank Ivo, Tijmen, Jaap and all the other guys from the club. Despite me being abroad for the past 7 years, have not forgotten about me and are always available for a beer when I am back home. I also appreciated the many visits they have paid me during my adventures abroad.

Special thanks to Myriam for all the love and support. I appreciate your intelligence, sense of humour and kind heart. I fondly look back at our adventures and hope for many more to come in the future.

I would like to dedicate this thesis to my grandparents. Unfortunately, my maternal grandparents both have passed away during the course of my PhD, but they have been of invaluable support while they were still around. They have had an immeasurable impact on the person I have become and I miss them dearly.

I would also like to thank my parents for putting up with me for all these years and giving me unconditional love and support. Thank you for nurturing my curiosity from when I was young and giving their all to help me succeed in life.

I would like to thank my brother, who has always been someone that inspired me and I looked up to. Thanks for being a great brother to me.

# 9. References


1. Genming, L. *et al.* Rapid oxygenation of Earth's atmosphere 2.33 billion years ago. *Sci. Adv.* **2**, e1600134 (2021).

2. Zachar, I. & Szathmáry, E. Breath-giving cooperation: critical review of origin of mitochondria hypotheses. *Biol. Direct* **12**, 19 (2017).

3. Becker, T. & Wagner, R. Mitochondrial outer membrane channels: emerging diversity in transport processes. *BioEssays* **40**, 1800013 (2018).

4. Boguszewska, K., Szewczuk, M., Kaźmierczak-Barańska, J. & Karwowski, B. T. The similarities between human mitochondria and bacteria in the context of structure, genome, and base excision repair system. *Molecules* **25**, 2857 (2020).

5. Plaitakis, A., Kalef-Ezra, E., Kotzamani, D., Zaganas, I. & Spanaki, C. The Glutamate Dehydrogenase Pathway and Its Roles in Cell and Tissue Biology in Health and Disease. *Biology (Basel).* **6**, 11 (2017).

6. Rasheed, M. R. H. Al & Tarjan, G. Succinate dehydrogenase complex: an updated review. *Arch. Pathol. Lab. Med.* **142**, 1564–1570 (2018).

7. Jitrapakdee, S. *et al.* Structure, mechanism and regulation of pyruvate carboxylase. *Biochem. J.* **413**, 369–387 (2008).

8. Imlay, J. A. Iron-sulphur clusters and the problem with oxygen. *Mol. Microbiol.* **59**, 1073–1082 (2006).

9. Guerra, G., Martínez, F. & Pardo, J. P. On the H+/2e− stoichiometry of the respiratory chain *. *Biochem. Mol. Biol. Educ.* **30**, 363–367 (2002).

10. Mårten, W. & Gerhard, H. Stoichiometry of proton translocation by respiratory complex I and its mechanistic implications. *Proc. Natl. Acad. Sci.* **109**, 4431–4436 (2012).

11. Nath, S. & Villadsen, J. Oxidative phosphorylation revisited. *Biotechnol. Bioeng.* **112**, 429–437 (2015).

12. Watt, I. N., Montgomery, M. G., Runswick, M. J., Leslie, A. G. W. & Walker, J. E. Bioenergetic cost of making an adenosine triphosphate molecule in animal mitochondria. *Proc. Natl. Acad. Sci.* **107**, 16823–16827 (2010).

13. Kaludercic, N. & Di Lisa, F. The energetic cost of NNT-dependent ROS removal. *J. Biol. Chem.* **295**, 16217–16218 (2020).

14. Zhao, R., Jiang, S., Zhang, L. & Yu, Z. Mitochondrial electron transport chain, ROS generation and uncoupling (Review). *Int J Mol Med* **44**, 3–15 (2019).

15. Muller, F. The nature and mechanism of superoxide production by the electron transport chain: Its relevance to aging. *J. Am. Aging Assoc.* **23**, 227–253 (2000).

16. Fujii, J., Homma, T. & Osaki, T. Superoxide Radicals in the Execution of Cell Death. *Antioxidants* **11**, 501 (2022).

17. Gutteridge, J. M. C. Iron promoters of the Fenton reaction and lipid peroxidation can be released from haemoglobin by peroxides. *FEBS Lett.* **201**, 291–295 (1986).

18. Battin, E. E. & Brumaghim, J. L. Antioxidant activity of sulfur and selenium: a review of reactive oxygen species scavenging, glutathione peroxidase, and metal-binding

antioxidant mechanisms. *Cell Biochem. Biophys.* **55**, 1–23 (2009).

19. Liu, D. & Zhang, F. Metabolic Feedback Circuits Provide Rapid Control of Metabolite Dynamics. *ACS Synth. Biol.* **7**, 347–356 (2018).

20. Simmen, F. A., Alhallak, I. & Simmen, R. C. M. Malic enzyme 1 (ME1) in the biology of cancer: it is not just intermediary metabolism. *J. Mol. Endocrinol.* **65**, R77–R90 (2020).

21. Lu, S. C. Glutathione synthesis. *Biochim. Biophys. Acta* **1830**, 3143–3153 (2013).

22. Zhang, H.-F., Klein Geltink, R. I., Parker, S. J. & Sorensen, P. H. Transsulfuration, minor player or crucial for cysteine homeostasis in cancer. *Trends Cell Biol.* (2022). doi:https://doi.org/10.1016/j.tcb.2022.02.009

23. Cole, S. P. C. & Deeley, R. G. Transport of glutathione and glutathione conjugates by MRP1. *Trends Pharmacol. Sci.* **27**, 438–446 (2006).

24. Banjac, A. *et al.* The cystine/cysteine cycle: a redox cycle regulating susceptibility versus resistance to cell death. *Oncogene* **27**, 1618–1628 (2008).

25. Errasti-Murugarren, E. & Palacín, M. Heteromeric amino acid transporters in brain: From physiology to pathology. *Neurochem. Res.* 1–14 (2021).

26. Palacín, M., Fernaández, E., Chillarón, J. & Zorzano, A. The amino acid transport system bo,+ and cystinuria. *Mol. Membr. Biol.* **18**, 21–26 (2001).

27. Sahota, A., Tischfield, J. A., Goldfarb, D. S., Ward, M. D. & Hu, L. Cystinuria: genetic aspects, mouse models, and a new approach to therapy. *Urolithiasis* **47**, 57–66 (2019).

28. Lewerenz, J. *et al.* The Cystine/Glutamate Antiporter System xc— in Health and Disease: From Molecular Mechanisms to Novel Therapeutic Opportunities. *Antioxid. Redox Signal.* **18**, 522–555 (2012).

29. Lequeux, A. *et al.* Targeting HIF-1 alpha transcriptional activity drives cytotoxic immune effector cells into melanoma and improves combination immunotherapy. *Oncogene* (2021). doi:10.1038/s41388-021-01846-x

30. Kang, R., Kroemer, G. & Tang, D. The tumor suppressor protein p53 and the ferroptosis network. *Free Radic. Biol. Med.* **133**, 162–168 (2019).

31. Liu, M., Zhu, W. & Pei, D. System Xc—: a key regulatory target of ferroptosis in cancer. *Invest. New Drugs* **39**, 1123–1131 (2021).

32. Piani, D. & Fontana, A. Involvement of the cystine transport system xc- in the macrophage-induced glutamate-dependent cytotoxicity to neurons. *J. Immunol.* **152**, 3578 LP – 3585 (1994).

33. Dong, X., Wang, Y. & Qin, Z. Molecular mechanisms of excitotoxicity and their relevance to pathogenesis of neurodegenerative diseases. *Acta Pharmacol. Sin.* **30**, 379–387 (2009).

34. Okazaki, S. *et al.* Glutaminolysis-related genes determine sensitivity to xCT-targeted therapy in head and neck squamous cell carcinoma. *Cancer Sci.* **110**, 3453–3463 (2019).

35. Liu, X., Zhang, Y., Zhuang, L., Olszewski, K. & Gan, B. NADPH debt drives redox bankruptcy: SLC7A11/xCT-mediated cystine uptake as a double-edged sword in cellular redox regulation. *Genes Dis.* **8**, 731–745 (2021).

36. Yu, X. & Long, Y. C. Crosstalk between cystine and glutathione is critical for the regulation of amino acid signaling pathways and ferroptosis. *Sci. Rep.* **6**, 30033 (2016).

37. Kilberg, M. S., Shan, J. & Su, N. ATF4-dependent transcription mediates signaling of amino acid limitation. *Trends Endocrinol. Metab.* **20**, 436–443 (2009).

38. Brouwers, B. *et al.* Loss of <em>Furin</em> in β-Cells Induces an mTORC1-ATF4 Anabolic Pathway That Leads to β-Cell Dysfunction. *Diabetes* **70**, 492 LP – 503 (2021).

39. Nomura, Y. *et al.* Characterization of the 5′-flanking region of the human and mouse CHAC1 genes. *Biochem. Biophys. Reports* **24**, 100834 (2020).

40. Gansemer, E. R. *et al.* NADPH and Glutathione Redox Link TCA Cycle Activity to Endoplasmic Reticulum Homeostasis. *iScience* **23**, 101116 (2020).

41. Wellen, K. E. & Thompson, C. B. Cellular metabolic stress: considering how cells respond to nutrient excess. *Mol. Cell* **40**, 323–332 (2010).

42. Roach, P. J. *et al.* Novel aspects of the regulation of glycogen storage. *J. Basic Clin. Physiol. Pharmacol.* **9**, 139–152 (1998).

43. Cao, J. Y. & Dixon, S. J. Mechanisms of ferroptosis. *Cell. Mol. Life Sci.* **73**, 2195–2209 (2016).

44. Magni, P. *et al.* Feeding behavior in mammals including humans. *Ann. N. Y. Acad. Sci.* **1163**, 221–232 (2009).

45. Schwartz, M. W., Woods, S. C., Porte, D., Seeley, R. J. & Baskin, D. G. Central nervous system control of food intake. *Nature* **404**, 661–671 (2000).

46. Mandel, I. D. The functions of saliva. *J. Dent. Res.* **66**, 623–627 (1987).

47. Gamble, J. L. & McIver, M. A. Acid-base composition of pancreatic juice and bile. *J. Exp. Med.* **48**, 849 (1928).

48. Kiela, P. R. & Ghishan, F. K. Physiology of Intestinal Absorption and Secretion. *Best Pract. Res. Clin. Gastroenterol.* **30**, 145–159 (2016).

49. Liu, R. *et al.* Gut microbiome and serum metabolome alterations in obesity and after weight-loss intervention. *Nat. Med.* **23**, 859 (2017).

50. Bouter, K. E., van Raalte, D. H., Groen, A. K. & Nieuwdorp, M. Role of the gut microbiome in the pathogenesis of obesity and obesity-related metabolic dysfunction. *Gastroenterology* **152**, 1671–1678 (2017).

51. Catanzaro, R. *et al.* The gut microbiota and its correlations with the central nervous system disorders. *Panminerva Med.* **57**, 127–143 (2014).

52. Grabacka, M., Pierzchalska, M., Dean, M. & Reiss, K. Regulation of ketone body metabolism and the role of PPARα. *Int. J. Mol. Sci.* **17**, 2093 (2016).

53. Ahmed, A., Wong, R. J. & Harrison, S. A. Nonalcoholic Fatty Liver Disease Review: Diagnosis, Treatment, and Outcomes. *Clin. Gastroenterol. Hepatol.* **13**, 2062–2070 (2015).

54. Ragbirsingh, Z. & Dhanoo, A. S. A History of Diabetes Mellitus.

55. Imbeault, P., Ravanelli, N. & Chevrier, J. Can POPs be substantially popped out

through sweat? *Environ. Int.* **111**, 131–132 (2018).

56. Baker, L. B. Physiology of sweat gland function: The roles of sweating and sweat composition in human health. *Temperature* **6**, 211–259 (2019).

57. Moore, J. W. The end of the road? Agricultural revolutions in the capitalist world-ecology, 1450–2010. *J. Agrar. Chang.* **10**, 389–413 (2010).

58. Cornier, M.-A. *et al.* The Metabolic Syndrome. *Endocr. Rev.* **29**, 777–822 (2008).

59. Echouffo-Tcheugui, J. B. & Selvin, E. Prediabetes and What It Means: The Epidemiological Evidence. *Annu. Rev. Public Health* **42**, 59–77 (2021).

60. Włodarczyk, M. & Nowicka, G. Obesity, DNA damage, and development of obesity-related diseases. *Int. J. Mol. Sci.* **20**, 1146 (2019).

61. Travis, J. On the origin of the immune system. (2009).

62. Ginhoux, F. & Jung, S. Monocytes and macrophages: developmental pathways and tissue homeostasis. *Nat. Rev. Immunol.* **14**, 392–404 (2014).

63. Jane, W.-E. M. Nutrition, the visceral immune system, and the evolutionary origins of pathogenic obesity. *Proc. Natl. Acad. Sci.* **116**, 723–731 (2019).

64. Hosogai, N. *et al.* Adipose tissue hypoxia in obesity and its impact on adipocytokine dysregulation. *Diabetes* **56**, 901–911 (2007).

65. Lee, Y. S. *et al.* Increased adipocyte O2 consumption triggers HIF-1α, causing inflammation and insulin resistance in obesity. *Cell* **157**, 1339–1352 (2014).

66. Schödel, J. & Ratcliffe, P. J. Mechanisms of hypoxia signalling: new implications for nephrology. *Nat. Rev. Nephrol.* **15**, 641–659 (2019).

67. Tannahill, G. M. *et al.* Succinate is an inflammatory signal that induces IL-1β through HIF-1α. *Nature* **496**, 238–242 (2013).

68. Jaitin, D. A. *et al.* Lipid-Associated Macrophages Control Metabolic Homeostasis in a Trem2-Dependent Manner. *Cell* **178**, 686-698.e14 (2019).

69. Luo, X., Wu, J., Jing, S. & Yan, L.-J. Hyperglycemic Stress and Carbon Stress in Diabetic Glucotoxicity. *Aging Dis.* **7**, 90–110 (2016).

70. Sparvero, L. J. *et al.* RAGE (Receptor for Advanced Glycation Endproducts), RAGE ligands, and their role in cancer and inflammation. *J. Transl. Med.* **7**, 1–21 (2009).

71. Khan, A. & Pessin, J. Insulin regulation of glucose uptake: a complex interplay of intracellular signalling pathways. *Diabetologia* **45**, 1475–1483 (2002).

72. Guilherme, A., Virbasius, J. V, Puri, V. & Czech, M. P. Adipocyte dysfunctions linking obesity to insulin resistance and type 2 diabetes. *Nat. Rev. Mol. cell Biol.* **9**, 367–377 (2008).

73. Yaribeygi, H., Farrokhi, F. R., Butler, A. E. & Sahebkar, A. Insulin resistance: Review of the underlying molecular mechanisms. *J. Cell. Physiol.* **234**, 8152–8161 (2019).

74. Pearson, E. R. Type 2 diabetes: a multifaceted disease. *Diabetologia* **62**, 1107–1112 (2019).

75. Gould, G. W. & Holman, G. D. The glucose transporter family: structure, function and tissue-specific expression. *Biochem. J.* **295**, 329 (1993).

76. Matschinsky, F. M. & Wilson, D. F. The Central Role of Glucokinase in Glucose Homeostasis: A Perspective 50 Years After Demonstrating the Presence of the Enzyme in Islets of Langerhans . *Frontiers in Physiology* **10**, 148 (2019).

77. Ježek, P. *et al.* The Pancreatic β-Cell: The Perfect Redox System. *Antioxidants* **10**, (2021).

78. Steiner, D. J., Kim, A., Miller, K. & Hara, M. Pancreatic islet plasticity: interspecies comparison of islet architecture and composition. *Islets* **2**, 135–145 (2010).

79. Ehses, J. A. *et al.* Increased Number of Islet-Associated Macrophages in Type 2 Diabetes. *Diabetes* **56**, 2356–2370 (2007).

80. Roscioni, S. S., Migliorini, A., Gegg, M. & Lickert, H. Impact of islet architecture on β-cell heterogeneity, plasticity and function. *Nat. Rev. Endocrinol.* **12**, 695 (2016).

81. Muratore, M., Santos, C. & Rorsman, P. The vascular architecture of the pancreatic islets: A homage to August Krogh. *Comp. Biochem. Physiol. Part A Mol. Integr. Physiol.* **252**, 110846 (2021).

82. Voorbij, H. A. M., Jeucken, P. H. M., Kabel, P. J., Haan, M. De & Drexhage, H. A. Dendritic cells and scavenger macrophages in pancreatic islets of prediabetic BB rats. *Diabetes* **38**, 1623–1629 (1989).

83. Gao, H. *et al.* Accumulation of microbial DNAs promotes to islet inflammation and β cell abnormalities in obesity in mice. *Nat. Commun.* **13**, 565 (2022).

84. Dror, E. *et al.* Postprandial macrophage-derived IL-1β stimulates insulin, and both synergistically promote glucose disposal and inflammation. *Nat. Immunol.* **18**, 283–292 (2017).

85. Böni-Schnetzler, M. & Meier, D. T. Islet inflammation in type 2 diabetes. in *Seminars in immunopathology* **41**, 501–513 (Springer, 2019).

86. Ying, W. *et al.* Expansion of Islet-Resident Macrophages Leads to Inflammation Affecting β Cell Proliferation and Function in Obesity. *Cell Metab.* **29**, 457-474.e5 (2019).

87. Nackiewicz, D. *et al.* Islet macrophages shift to a reparative state following pancreatic beta-cell death and are a major source of islet insulin-like growth factor-1. *Iscience* **23**, 100775 (2020).

88. Eguchi, K. *et al.* Saturated fatty acid and TLR signaling link β cell dysfunction and islet inflammation. *Cell Metab.* **15**, 518–533 (2012).

89. Corbett, J. A. & McDaniel, M. L. Intraislet release of interleukin 1 inhibits beta cell function by inducing beta cell expression of inducible nitric oxide synthase. *J. Exp. Med.* **181**, 559–568 (1995).

90. Kolliniati, O., Ieronymaki, E., Vergadi, E. & Tsatsanis, C. Metabolic Regulation of Macrophage Activation. *J. Innate Immun.* (2021). doi:10.1159/000516780

91. Verberk, S. G. S., de Goede, K. E. & Van den Bossche, J. Metabolic–epigenetic crosstalk in macrophage activation: an updated view. *Epigenomics* **11**, 719–721 (2019).

92. He, W., Heinz, A., Jahn, D. & Hiller, K. Complexity of macrophage metabolism in infection. *Curr. Opin. Biotechnol.* **68**, 231–239 (2021).

93. Du, Y. *et al.* Lysine malonylation is elevated in type 2 diabetic mouse models and

enriched in metabolic associated proteins. *Mol. Cell. Proteomics* **14**, 227–236 (2015).

94. Galván-Peña, S. *et al.* Malonylation of GAPDH is an inflammatory signal in macrophages. *Nat. Commun.* **10**, 1–11 (2019).

95. O'Neill, L. A. J. & Artyomov, M. N. Itaconate: the poster child of metabolic reprogramming in macrophage function. *Nat. Rev. Immunol.* **19**, 273–281 (2019).

96. Littlewood-Evans, A. *et al.* GPR91 senses extracellular succinate released from inflammatory macrophages and exacerbates rheumatoid arthritis. *J. Exp. Med.* **213**, 1655–1662 (2016).

97. Diskin, C. & Pålsson-McDermott, E. M. Metabolic Modulation in Macrophage Effector Function. *Front. Immunol.* **9**, 270 (2018).

98. Lewerenz, J. *et al.* The cystine/glutamate antiporter system x(c)(-) in health and disease: from molecular mechanisms to novel therapeutic opportunities. *Antioxid. Redox Signal.* **18**, 522–555 (2013).

99. Hsieh, C.-H. *et al.* HIF-1α triggers long-lasting glutamate excitotoxicity via system x(c)(-) in cerebral ischaemia-reperfusion. *J. Pathol.* **241**, 337–349 (2017).

100. Evonuk, K. S. *et al.* Inhibition of system Xc− transporter attenuates autoimmune inflammatory demyelination. *J. Immunol.* **195**, 450–463 (2015).

101. Arntfield, M. E. & van der Kooy, D. β-Cell evolution: How the pancreas borrowed from the brain: The shared toolbox of genes expressed by neural and pancreatic endocrine cells may reflect their evolutionary relationship. *Bioessays* **33**, 582–587 (2011).

102. Maechler, P. Glutamate pathways of the beta-cell and the control of insulin secretion. *Diabetes Res. Clin. Pract.* **131**, 149–153 (2017).

103. Huang, X.-T. *et al.* An excessive increase in glutamate contributes to glucose-toxicity in β-cells via activation of pancreatic NMDA receptors in rodent diabetes. *Sci. Rep.* **7**, 44120 (2017).

104. Brykczynska, U. *et al.* Distinct transcriptional responses across tissue-resident macrophages to short-term and long-term metabolic challenge. *Cell Rep.* **30**, 1627–1643 (2020).

105. Sato, H. *et al.* Redox imbalance in cystine/glutamate transporter-deficient mice. *J. Biol. Chem.* **280**, 37423–37429 (2005).

106. Teskey, G. *et al.* Glutathione as a marker for human disease. *Adv. Clin. Chem.* **87**, 141–159 (2018).

107. Midha, A. *et al.* Unique Human and Mouse β-Cell Senescence-Associated Secretory Phenotype (SASP) Reveal Conserved Signaling Pathways and Heterogeneous Factors. *Diabetes* **70**, 1098–1116 (2021).

108. Pi, J. *et al.* Reactive oxygen species as a signal in glucose-stimulated insulin secretion. *Diabetes* **56**, 1783–1791 (2007).

109. Bruni, A. *et al.* Ferroptosis-inducing agents compromise in vitro human islet viability and function. *Cell Death Dis.* **9**, 595 (2018).

110. Shi, Z., Naowarojna, N., Pan, Z. & Zou, Y. Multifaceted mechanisms mediating cystine starvation-induced ferroptosis. *Nat. Commun.* **12**, 4792 (2021).

111. Held, J. M. Redox Systems Biology: Harnessing the Sentinels of the Cysteine Redoxome. *Antioxid. Redox Signal.* **32**, 659–676 (2020).

112. Bonifácio, V. D. B., Pereira, S. A., Serpa, J. & Vicente, J. B. Cysteine metabolic circuitries: druggable targets in cancer. *Br. J. Cancer* **124**, 862–879 (2021).

113. Hanigan, M. H. Gamma-glutamyl transpeptidase: redox regulation and drug resistance. *Adv. Cancer Res.* **122**, 103–141 (2014).

114. Ardestani, A., Lupse, B., Kido, Y., Leibowitz, G. & Maedler, K. mTORC1 Signaling: A Double-Edged Sword in Diabetic β Cells. *Cell Metab.* **27**, 314–331 (2018).

115. Xiao, W. & Loscalzo, J. Metabolic responses to reductive stress. *Antioxid. Redox Signal.* **32**, 1330–1347 (2020).

116. Gu, Y. *et al.* mTORC2 Regulates Amino Acid Metabolism in Cancer by Phosphorylation of the Cystine-Glutamate Antiporter xCT. *Mol. Cell* **67**, 128-138.e7 (2017).

117. Ishimoto, T. *et al.* CD44 variant regulates redox status in cancer cells by stabilizing the xCT subunit of system xc− and thereby promotes tumor growth. *Cancer Cell* **19**, 387–400 (2011).

118. Kobayashi, N. *et al.* CD44 variant inhibits insulin secretion in pancreatic β cells by attenuating LAT1-mediated amino acid uptake. *Sci. Rep.* **8**, 2785 (2018).

119. Bachhawat, A. K. & Kaur, A. Glutathione Degradation. *Antioxid. Redox Signal.* **27**, 1200–1216 (2017).

120. Van Liefferinge, J. *et al.* Comparative analysis of antibodies to xCT (Slc7a11): Forewarned is forearmed. *J. Comp. Neurol.* **524**, 1015–1032 (2016).

121. Lee, Y. S. & Olefsky, J. Chronic tissue inflammation and metabolic disease. *Genes Dev.* **35**, 307–328 (2021).

122. Lee, J. Adipose tissue macrophages in the development of obesity-induced inflammation, insulin resistance and type 2 diabetes. *Arch. Pharm. Res.* **36**, 208–222 (2013).

123. A., H. D. *et al.* Distinct macrophage populations direct inflammatory versus physiological changes in adipose tissue. *Proc. Natl. Acad. Sci.* **115**, E5096–E5105 (2018).

124. Dixon, S. J. & Stockwell, B. R. The hallmarks of ferroptosis. *Annu. Rev. Cancer Biol.* **3**, 35–54 (2019).

125. Stamatiades, G. A., Echouffo-Tcheugui, J. B. & Garber, J. R. Sulfasalazine-Induced Hypoglycemia in a Patient with Type 2 Diabetes and End-Stage Renal Disease. *AACE Clin. Case Reports* **4**, e493–e496 (2018).

126. Collins, S. L. *et al.* mTORC1 signaling regulates proinflammatory macrophage function and metabolism. *J. Immunol.* **207**, 913–922 (2021).

127. Lopez-Castejon, G. & Brough, D. Understanding the mechanism of IL-1β secretion. *Cytokine Growth Factor Rev.* **22**, 189–195 (2011).

128. Murray, R. Z. & Stow, J. L. Cytokine Secretion in Macrophages: SNAREs, Rabs, and Membrane Trafficking . *Frontiers in Immunology* **5**, (2014).

129. Min, B.-K. *et al.* Pyruvate Dehydrogenase Kinase Is a Metabolic Checkpoint for

Polarization of Macrophages to the M1 Phenotype. *Front. Immunol.* **10**, 944 (2019).

130. D., A. M. *et al.* Cystine–glutamate antiporter xCT deficiency suppresses tumor growth while preserving antitumor immunity. *Proc. Natl. Acad. Sci.* **116**, 9533–9542 (2019).

131. Marquard, J. *et al.* Characterization of pancreatic NMDA receptors as possible drug targets for diabetes treatment. *Nat. Med.* **21**, 363–372 (2015).

132. Teselkin, Y. O. *et al.* Combined Effect of TLR2 Ligands on ROS Production by Mouse Peritoneal Macrophages. *Bull. Exp. Biol. Med.* **166**, 26–30 (2018).

133. Dalmas, E. *et al.* Interleukin-33-activated islet-resident innate lymphoid cells promote insulin secretion through myeloid cell retinoic acid production. *Immunity* **47**, 928–942 (2017).